INTERNATIONAL ATOMIC ENERGY AGENCY
UNITED NATIONS EDUCATIONAL, SCIENTIFIC AND CULTURAL ORGANIZATION

INTERNATIONAL CENTRE FOR THEORETICAL PHYSICS
34100 TRIESTE (ITALY) - P.O.B. 586 - MIRAMARE - STRADA COSTIERA 11 - TELEPHONE: 2240-1
CABLE: CENTRATOM - TELEX 460392 - I

SMR/208 - 17

SPRING COLLEGE IN MATERIALS SCIENCE

ON

"METALLIC MATERIALS"

(11 May - 19 June 1987)

DISLOCATIONS
(Part III)

J.Th.M. DE HOSSON
Department of Applied Physics
University of Groningen
9747 AG Groningen
The Netherlands

Reprinted from

ACTA METALLURGICA

Vol. 32, *No.* 8, *pp.* 1205–1215

DISLOCATION DYNAMICS IN Al–Li ALLOYS. MEAN JUMP DISTANCE AND ACTIVATION LENGTH OF MOVING DISLOCATIONS

J. TH M. DE HOSSON,[1] A. HUIS IN'T VELD,[1] H. TAMLER[2] and O. KANERT[2]

[1]Department of Applied Physics, Materials Science Centre, University of Groningen, Nijenborgh 18, 9747 AG Groningen, The Netherlands and [2]Institute of Physics, University of Dortmund, 46 Dortmund 50, F.R.G.

PERGAMON PRESS
OXFORD · NEW YORK · TORONTO · SYDNEY
PARIS · FRANKFURT
1984

Acta metall. Vol. 32, No. 8, pp. 1205–1215, 1984
Printed in Great Britain.

0001-6160/84 $3.00 + 0.00

DISLOCATION DYNAMICS IN Al–Li ALLOYS. MEAN JUMP DISTANCE AND ACTIVATION LENGTH OF MOVING DISLOCATIONS

J. Th M. De HOSSON, A. HUIS in't VELD

Department of Applied Physics, Materials Science Centre, University of Groningen, Nijenborgh 18, 9747 AG Groningen, The Netherlands

and

H. TAMLER, O. KANERT

Institute of Physics, University of Dortmund, 46 Dortmund 50, F.R.G.

(*Received* 19 *January* 1984)

Abstract—Pulsed nuclear magnetic resonance proved to be a complementary new technique for the study of moving dislocations in Al–Li alloys. The NMR technique in combination with transmission electron microscopy and strain-rate change experiments have been applied to study dislocation motion in Al–2.2 wt% Li alloys, aged at 215°C (1 h) and 245°C (115 h). These heat treatments were chosen in order to obtain considerable differences in particle sizes which influence the mechanical properties. From the motion-induced part of the spin lattice relaxation rate, $T_{1\rho}^{-1}$ of ^{27}Al the mean jump distance of mobile dislocations has been measured as a function of strain. Transmission electron microscopic observations of the mean planar diameter of δ' precipitates, together with the NMR data, predicted the increase in yield stress of these alloys compared to ultrapure Al in agreement with experiments. In alloys aged 1 h at 215°C the precipitates are believed to be shearable. After aging 115 h at 245°C NMR and TEM observations indicated that the particles were not sheared. It was found that the activation length, obtained from mechanical strain-rate change experiments have different values compared to the values of the mean jump distance determined by NMR. Reasons for the mean jump distance being different from the activation length have been given. Nevertheless, there exists an internal consistency, namely: both mean jump distance and activation length have been found to decrease with strain hardening more rapidly in Al–Li containing nonshearable precipitates than in Al–Li containing shearable precipitates.

Résumé—La résonance magnétique nucléaire pulsée est une nouvelle technique complémentaire pour l'étude des dislocations en déplacement dans des alliages Al–Li. Nous avons utilisé la RMN, ainsi que la microscopie électronique en transmission et des expériences de changement de la vitesse de déformation pour étudier le déplacement des dislocations dans des alliages Al–2,2% Li (en poids) vieillis à 215°C (1 h) et à 245°C (115 h). Nous avons choisi ces traitements thermiques afin d'obtenir des différences considérables dans les tailles de particules, qui influencent les propriétés mécaniques. Nous avons mesuré la distance de saut moyenne pour les dislocations mobiles en fonction de la déformation à partir de la partie de la vitesse de relaxation spin-réseau de ^{27}Al induite par le mouvement $T_{1\rho}^{-1}$. Des observations du diamètre planaire moyen des précipités δ' par microscopie électronique en transmission, associées aux résultats de la RMN, ont permis de prévoir l'accroissement de la limite élastique de ces alliages par rapport à l'aluminium ultrapur, en accord avec les expériences. Dans les alliages vieillis 1 h à 215°C, nous pensons que les précipités peuvent être cisaillés. Après vieillissement de 115 h à 245°C, la RMN et la MET ont montré que les particules n'étaient pas cisaillées les valeurs de la longueur d'activation, obtenues à partir des expériences de changement de la vitesse de déformation mécanique, étaient différentes des valeurs de la distance de saut moyenne déterminées par RMN. Nous proposons des explications pour cette différence entre les valeurs de la distance de saut moyenne et la longueur d'activation. Néanmoins, il existe une cohérence interne: la distance de saut moyenne et la longueur d'activation diminuent avec le durcissement plus rapidement dans Al–Li contenant des précipités non cisaillables que dans Al–Li contenant des précipités cisaillables.

Zusammenfassung—Gepulste Kernspinresonanz hat sich als eine neue ergänzende Meßmethode zur Untersuchung der Versetzungsbewegung in Al–Li erwiesen. Sie wurde zusammen mit des Durchstrahlungselektronenmikroskopie und mit Geschwindigkeitswechseln auf die Versetzungsbewegung in Al–2,2 Gew.-% Li, die bei 215°C für 1 h oder bei 245°C für 115 h ausgelagert worden waren, angewendet. Mit diesen Wärmebehandlungen wurden beträchtliche Unterschiede in den das mechanische Verhalten beeinflussende Teilchengrößen erhalten. Aus dem bewegungsinduzierten Teil der Spingitterrelaxationsrate $T_{1\rho}^{-1}$ des ^{27}Al wurde die mittlere Sprungweite der beweglichen Versetzungen in Abhängigkeit von der Dehnung gemessen. Durchstrahlungselektronenmikroskopische Beobachtungen der mittleren ebenen Durchmesser der δ'-Ausscheidungen ergaben zusammen mit den Kernspinresonanzmessungen eine erhöhte Fließspannung dieser Legierungen im Vergleich zu ultrareinem Al, in übereinstimmung mit den Experimenten. In den Legierungen mit einstündiger Auslagerung bei 215°C sind die Ausscheidungen wohl scherbar. Elektronenmikroskopie und Kernspinresonanz zeigen, daß sie nach Auslagerung bei 245°C für 115 h nicht geschert werden. Die Aktivierungslängen, die aus der mechanischen Geschwindigkeitswechselversuchen erhalten wurden, unterscheiden sich von den Sprunglängen aus der Kernspinresonanz. Gründe für diesen Unterschied werden angeführt. Nichtsdestoweniger gibt es eine innere Verträglichkeit: sowohl mittlere Sprungweite als auch Aktivierungslänge nehmen mit der Verfestigung rascher in Al–Li-Legierungen mit nicht-scherbaren Ausscheidungen ab als in Legierungen mit scherbaren Ausscheidungen.

1. INTRODUCTION

Aluminium–lithium based alloys offer considerable promise for structural applications, especially in aerospace industry [1], since they possess the potential for high strength in combination with a lower density and a higher modulus of elasticity than conventional aluminium alloys. The strengthening mechanism of Al–Li alloys is due to the formation of coherent δ' precipitates [2] (ordered $L1_2$ phase Al_3Li). To understand the strengthening mechanism we have investigated the way in which moving dislocations interact with precipitate particles of the coherent phase δ'. In this paper, a nuclear magnetic resonance study of the mechanism of dislocation motion in Al–2.2 wt% Li is reported. The *in situ* nuclear spin relaxation measurements provide information about the effective mean jump distance of mobile dislocations. In addition, the activation length of mobile dislocations has been obtained from strain-rate change experiments on Al-2.2 wt% Li. Both the mean jump distance and the activation length were related to the *static* transmission electron microscopic observations of the instantaneous configuration of dislocations and the precipitates. The experiments were carried out on Al–Li alloys aged at two different temperatures: 215 C (1 h) and 245 C (115 h). These heat treatments were chosen in order to obtain considerable differences in particle sizes which influence the mechanical properties and dislocation dynamics.

2. THEORETICAL BACKGROUND

A few years ago, we showed that pulsed nuclear magnetic resonance is a useful tool to study dislocation motion. It turned out that three sets of microscopic information about the dislocation motion can be deduced in principle from these experiments:

(i) the mean jump distance of moving dislocations.
(ii) the mean time of stay between two consecutive jumps of a mobile dislocation; and
(iii) the mobile dislocation density as a fraction of the total dislocation density.

While *static* quadrupolar effects associated with static lattice defects such as dislocations are analyzed in terms of width, line shape and intensity of the NMR signal, *dynamical* effects, such as dislocation motion during plastic deformation, are studied through the related nuclear spin-lattice relaxation process. Nevertheless, both experimental methods are essentially based on the interaction between nuclear electric quadrupole moments and electric field gradients at the nucleus. Around a dislocation in a cubic crystal the symmetry is destroyed and interactions between nuclear electric quadrupole moments and electric field gradients arise. Whenever a dislocation changes its position in the crystal, the surrounding atoms have also to move, thus causing time fluctuations both of the quadrupolar and dipolar spin Hamiltonian for spins with $I > \frac{1}{2}$. However, dipolar effects on the nuclear spin relaxation due to dislocation motion are negligible and quadrupolar interactions dominate the observed relaxation behaviour. Furthermore, for the investigation of rather infrequent defect motions as in the case of moving dislocations, the spin-lattice relaxation time in the rotating frame, $T_{1\rho}$, has proved to be the most appropriate NMR parameter affected by such motions. For detailed information of this technique reference is made to previous work [3–6]. Only a concise review will be given here.

While deforming a sample with a constant strain rate $\dot{\epsilon}$ the spin-lattice relaxation rate in a (weak rotating) applied field H_1, $(1/T_{1\rho})$ of the resonant nuclei in the sample is enhanced due to the motion of dislocations. The resulting expression for the relaxation rate induced by dislocation motion is given by

$$\left(\frac{1}{T_{1\rho}}\right)_D = \frac{A_Q}{H_1^2 + H_{L\rho}^2}\frac{\rho_m}{\tau_u} \tag{1}$$

where A_Q depends on the mean-squared electric field gradient due to the stress field of a dislocation of unit length and the quadrupolar coupling constant. $H_{L\rho}$ is the mean local field in the rotating frame determined by the local dipolar field $H_{D\rho}$ and the local quadrupolar field $H_{Q\rho}$. ρ_m and τ_u represent the mobile dislocation density and the waiting time of a mobile dislocation, respectively. The deformation experiments are carried out in a magnetic field of 1.4 T with a constant deformation rate $\dot{\epsilon}$. This type of experiment is governed by Orowan's equation [7]. Assuming a thermally activated jerky motion of mobile dislocations, the macroscopic strain rate is given by (steady state mobile density) [8]

$$\dot{\epsilon} = \phi b \rho_m L / \tau_m \tag{2}$$

where τ_m is the mean time of stay between successive jumps (waiting time τ_u plus actual jump time τ_j). b is the magnitude of the Burgers vector, ϕ is a geometrical factor, and L is the mean jump distance. Since $\tau_m \simeq \tau_u (\tau_j \ll \tau_u)$ follows for the spin lattice relaxation rate [equation (1)] using equation (2):

$$\left(\frac{1}{T_{1\rho}}\right)_D = \frac{A_Q}{H_1^2 + H_{L\rho}^2}\frac{1}{\phi b L}\dot{\epsilon}. \tag{3}$$

Hence, for a given plastic deformation rate $\dot{\epsilon}$ the nuclear spin relaxation rate is proportional to the inverse of the mean jump distance L. A_Q and $H_{L\rho}^2$ have been obtained separately from a line shape analysis of the NMR signal [9] and spin echo NMR measurements [10]. Relationship (3) has been used to determine L as a function of strain.

On the other hand, the strain rate can be written as [8]

$$\dot{\epsilon} = \dot{\epsilon}_0 \exp\left(-\frac{\Delta G}{kT}\right) \tag{4}$$

where ΔG is the activation energy for intersection, assuming that the only release of a dislocation segment from an obstacle is due to thermal fluctuations. The Arrhenius' type of behaviour of $\dot{\epsilon}$ holds for the asymptotic flow stress [11]. The apparent activation volume is defined as

$$V = -\left(\frac{\delta \Delta G}{\delta \tau}\right)_T = kT\left(\frac{\delta \ln \dot{\epsilon}}{\delta \tau}\right)_T \simeq \lambda b^2 \qquad (5)$$

where $\dot{\epsilon}_0$ is taken to be independent of the shear stress τ. λ represents the average obstacle spacing or the activated minimum length. Mechanical tests involving a change in strain rate by a factor of ten have been employed to measure $(\delta \ln \dot{\epsilon}/\delta \tau)_T$, equation (5), from which the apparent activation volume and average spacing λ have been deduced.

3. EXPERIMENTAL

Polycrystalline samples with a grain size of the order of 100–200 μm were used. To avoid skin effect distortion of the NMR signal the NMR experiments were carried out on rectangular foils of size 27 mm × 12 mm × 40 μm. The starting material for the Al–Li samples was Al–2.5 wt% Li. After a homogenizing procedure at 580 C for 1 h the material was rolled out to the aforementioned thickness and has then been cut by spark erosion to the sample size given above. Afterwards, the samples were annealed a second time at 580 C for 7 min and quenched in water. In order to produce δ' precipitates of different sizes the samples were exposed to a third heat treatment (either 1 h at 215 C or 115 h at 245 C). After the heat treatments, the Li content was measured by means of a Perkin–Elmer spectrophotometer and appeared to be equal to 2.2 wt%.

In the NMR experiment, the sample under investigation is plastically deformed by a servo-hydraulic tensile machine (ZONIC Technical Lab. Inc., Cincinnati) of which the exciter head XCI 1105 moves a driving rod with a constant velocity. While the specimen was deforming, ^{27}Al nuclear spin measurements were carried out by means of a BRUKER pulse spectrometer SXP 4-100 operating at 15.7 MHz corresponding to a magnetic field of 1.4 T controlled by an NMR stabilizer (BRUKER B-SN 15). The NMR head of the spectrometer and the frame in which the rod moves formed a unit which was inserted between the pole pieces of the electromagnet of the spectrometer. The set-up of the whole tensile testing system is described in [5]. A scheme of the experimental set-up is displayed in Fig. 1. As shown in this block diagram, the spectrometer was triggered by the electronic control of the tensile machine. The trigger starts the nuclear spin relaxation experiment at a definite time during the deformation determined by the delay time of the trigger pulse. Immediately before and after the plastic deformation the mag-

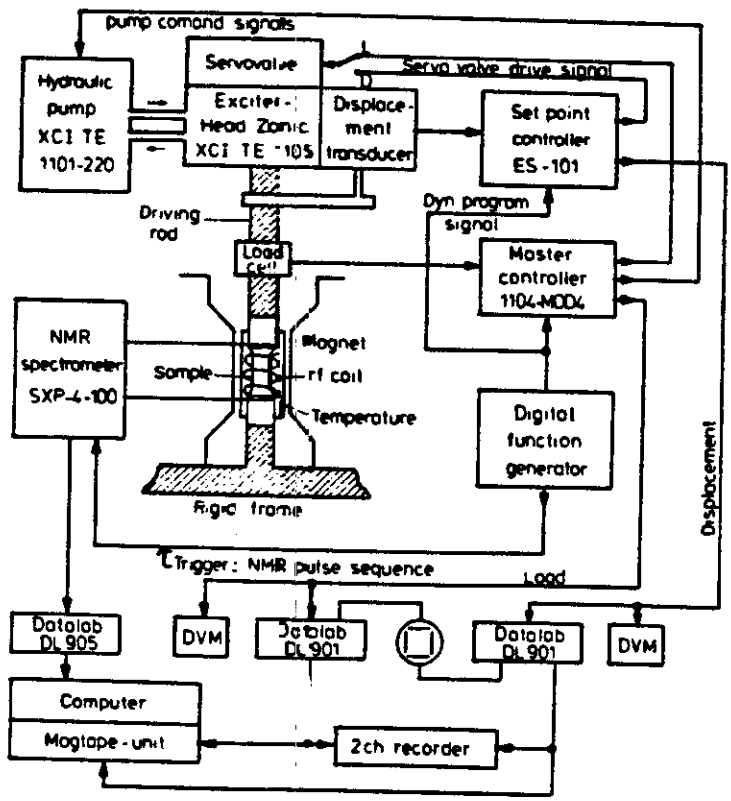

Fig. 1. Block scheme of the experimental set-up, consisting of the deformation equipment, NMR spectrometer and magnet, data recording and handling instruments.

nitude of the background (conduction-electron) relaxation time $(T_{1\rho})_0$ was measured. From the experimental $T_{1\rho}$-data, the dislocation induced contribution of the relaxation time, $(T_{1\rho})_D$, could be determined, according to

$$\frac{1}{T_{1\rho}} = \left(\frac{1}{T_{1\rho}}\right)_0 + \left(\frac{1}{T_{1\rho}}\right)_D. \tag{6}$$

To be sure that the increase in the nuclear spin relaxation rate during plastic deformation with $\dot{\epsilon}$ = constant is caused actually by internal atomic motions and not by any kind of external electrodynamic effects, $(T_{1\rho})^{-1}$ was measured while moving the whole sample with a constant velocity but without deformation. No change within experimental error in the relaxation rate was observed in such an experiment.

The NMR and mechanical measurements discussed here were carried out at 77 K. At such a low temperature nuclear spin relaxation effects due to diffusive atomic motions are negligible. Taking the Einstein–Smoluchowski equation as a starting point for connecting the diffusion coefficient with the mean time of stay τ_c of an atom between two diffusion jumps (neglecting correlation effects) the correlation times for atomic jumps of ^{27}Al and Li in the aluminium matrix can be calculated at 77 K. These calculations indicate that ^{27}Al and Li are actually immobile. The correlation times ($> 10^{-9}$ s) are much larger than typical values of τ_c for mobile dislocations ($\simeq 10^{-4}$ s with $\dot{\epsilon} \simeq 1\,\mathrm{s}^{-1}$). Consequently, an observable contribution of diffusive atomic motions to $T_{1\rho}$ does not occur.

Transmission electron micrographs were taken by using a JEM 200 CX operating between 120 and 160 kV. Disc-type specimens were obtained from the deformed foils by spark cutting to minimize deformation. The samples were electrochemically thinned in polishing equipment at room temperature in a solution of 49% methanol, 49% nitric acid, 2% hydrochloric acid. Dislocations were imaged in dark-field using the weak-beam technique [12].

4. RESULTS AND DISCUSSION

4.1. Mean jump distance

In Fig. 2 the mean jump distance measured by NMR in Al–Li aged at 215°C (1 h) is illustrated as a function of strain. The spin lattice relaxation rate was determined at a constant strain rate $\dot{\epsilon} = 1.6\,\mathrm{s}^{-1}$. The shape of the L vs ϵ curve is quite similar to the curve obtained for ultrapure Al using NMR techniques [4]. Apparently at the beginning of deformation the storage of dislocations follows strictly geometrical or statistical rules. Assuming that the mean jump distance is proportional to the slip line length Λ_L which decreases with increasing strain in pure f.c.c. metals, it means that

$$\frac{1}{L} \approx \epsilon. \tag{7}$$

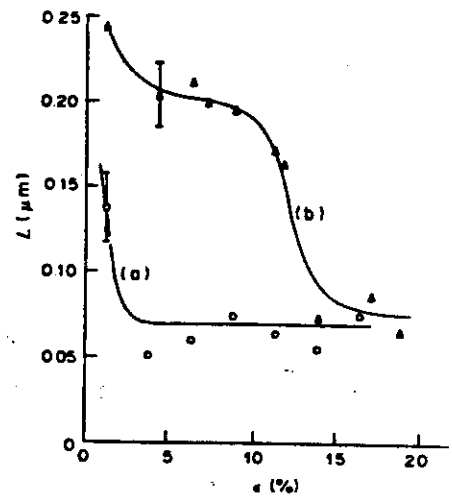

Fig. 2. The mean jump distance measured by NMR as a function of strain ϵ in (a) Al–2.2 wt% Li aged at 215°C (1 h) and (b) Al–2.2 wt% Li aged at 245 C (115 h). Each data point represents the averaged value over 5 measurements. The error bar indicates the deviation within a set of L-data at a particular ϵ ($\dot{\epsilon} = 1.6\,\mathrm{s}^{-1}$).

An electron micrograph illustrating the microstructure of deformed Al–Li till fracture is shown in Fig. 3. δ' superlattice reflections have been used for imaging the Al_3Li precipitates (dark field/strong beam, $\mathbf{g} = [001]$). The appearance of superlattice dislocations in this alloy shown in Fig. 4 (dark field/weak beam image) indicates that the precipitates are shearable. Stereo-electron micrographs revealed that the volume fraction f is about 3% and the mean diameter $2\bar{R}$ of the precipitates is about 15 nm leading to a Friedel spacing of 0.08 μm and a mean square spacing of 0.06 μm. The square lattice spacing of the particles is calculated from

$$L_s = \left(\frac{\pi}{f}\right)^{1/2} \bar{R}, \tag{8}$$

and the Friedel spacing is defined as [13]

$$L_F = \left(\frac{\pi T \bar{R}_s}{\gamma f}\right)^{1/2} \tag{9}$$

where T represents the line tension ($\simeq 0.5\,\mu b^2$, $\mu = 0.3 \cdot 10^5$ MPa) and $\bar{R}_s$ is the mean planar radius of the particles ($\pi/4\,\bar{R}$). From the separation between the two ordinary unit dislocations constituting a superlattice dislocation (96 nm in Fig. 4) an antiphase boundary energy $\gamma = 140\,\mathrm{mJ/m^2}$ has been found. Both values L_s and L_F are close to the mean jump distance L measured by NMR. However, the mean jump distance is much larger than the average particle diameter $\bar{d}$. Therefore, the δ' ordered precipitates are considered to be perfectly sheared off during deformation. If n dislocations of Burgers vector b shear a particle, then the cross section of the precipitate in the slip plane will be reduced by an amount nb. Consequently, the effective planar diameter of the particle can be considered to decrease as the strain increases. Since the flow stress is proportional to $(\bar{d})^{1/2}$ [14], the flow resistance on an identical slip plane decreases as

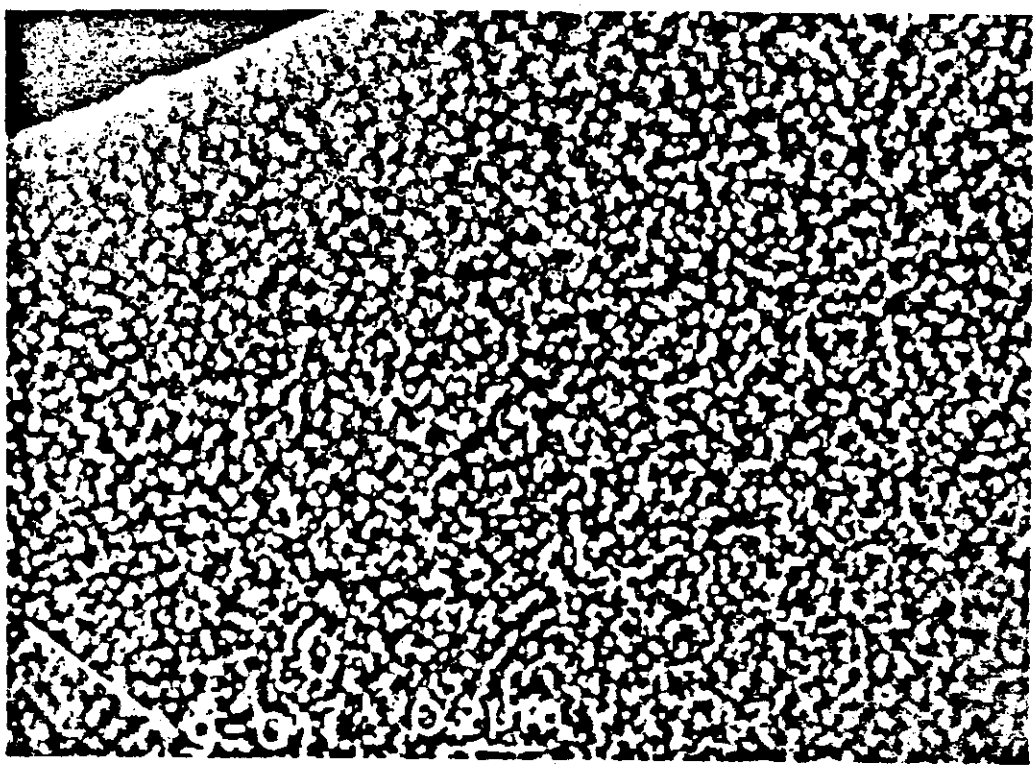

Fig. 3. Al–2.2 wt% Li aged at 215°C (1 h) deformed till fracture g = [01$\bar{1}$].

the strain increases. The slip plane is thus work-softened so that further slip will tend to concentrate on that plane. After the passage of some pairs of superlattice dislocations (which were only imaged in the electron microscope when $\epsilon \leqslant 5\%$) the ordered precipitates are finally sheared off completely. Then, *single* dislocations become easily mobile, leading to the formation of the arrays of pile-up dislocations

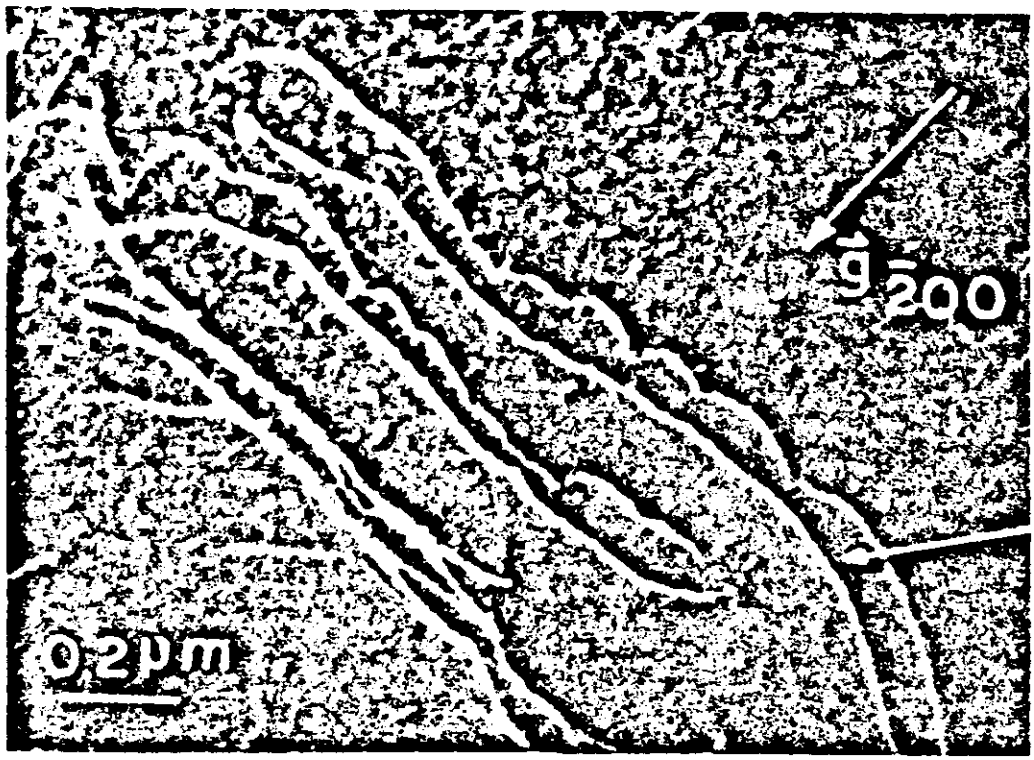

Fig. 4. Al–2.2 wt% Li aged at 215°C (1 h) deformed 5% at 77 K. Dark field weak beam image. [011] orientation. g = [200]. Superlattice dislocation imaged: $\frac{1}{2}$[101](1$\bar{1}$1)

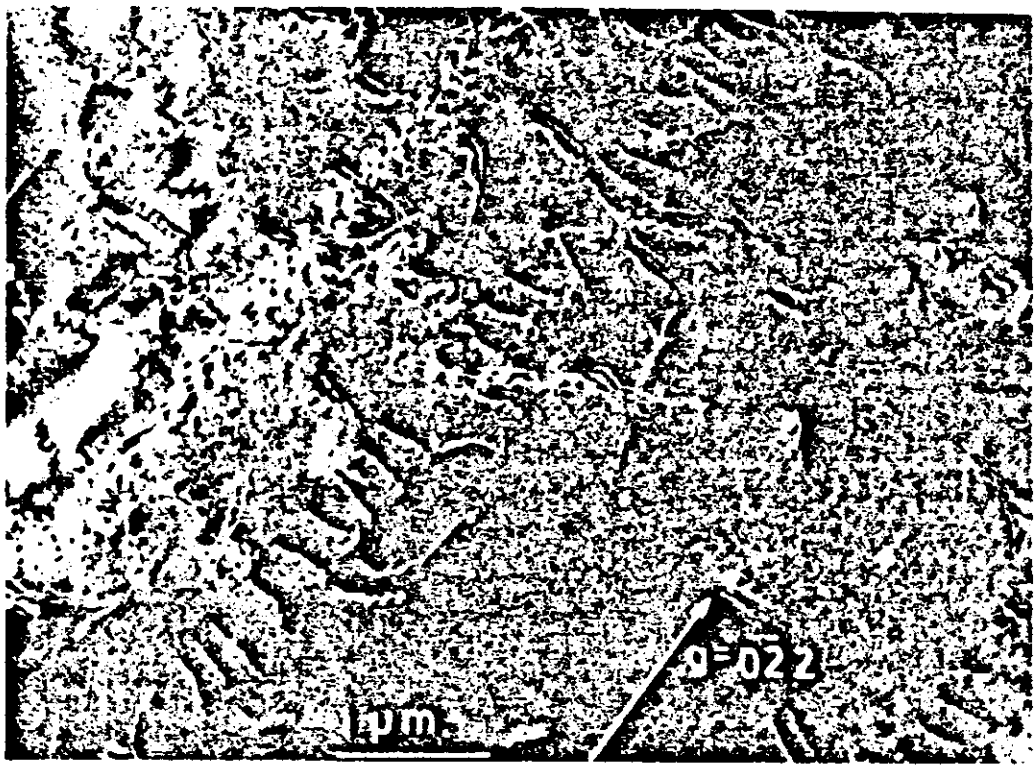

Fig. 5. A pile-up of coupled dislocations in Al–2.2 wt% Li aged at 215 C (1 h) deformed till fracture at 77 K. Dark field weak beam image, $\mathbf{g} = [0\bar{2}2]$.

(see Fig. 5) [15]. Near the head of the pile-up, the dislocations are obviously paired but the pair spacing increases for dislocations further toward the tail until after a number of dislocations they become uncoupled.

At aging temperatures above 230 C coarsening of the precipitates occurred. In Fig. 6 a stereo micrograph of an Al–Li sample (undeformed) aged at 230 C for 17 h is shown. By using two diffraction spots, namely a superlattice reflection and a matrix reflection, dislocations as well as precipitates are imaged. A row of δ' precipitates are preferentially nucleated on a matrix dislocation. After aging at 230 C collinear rows of extra large precipitates were observed, sometimes elongated along the line direction. In those cases a dislocation was found to be associated with the rows, lying on the common line between particles and on the surface of the particles themselves. This may be explained by pipe diffusion.

The mean jump distance of moving dislocations in Al–2.2 wt% Li aged at 245 C (115 h) as a function of strain is displayed in Fig. 2.

Figure 7 shows an electron micrograph (dark field/weak beam, $\mathbf{g} = [02\bar{2}]$) of the Al–Li alloy de-

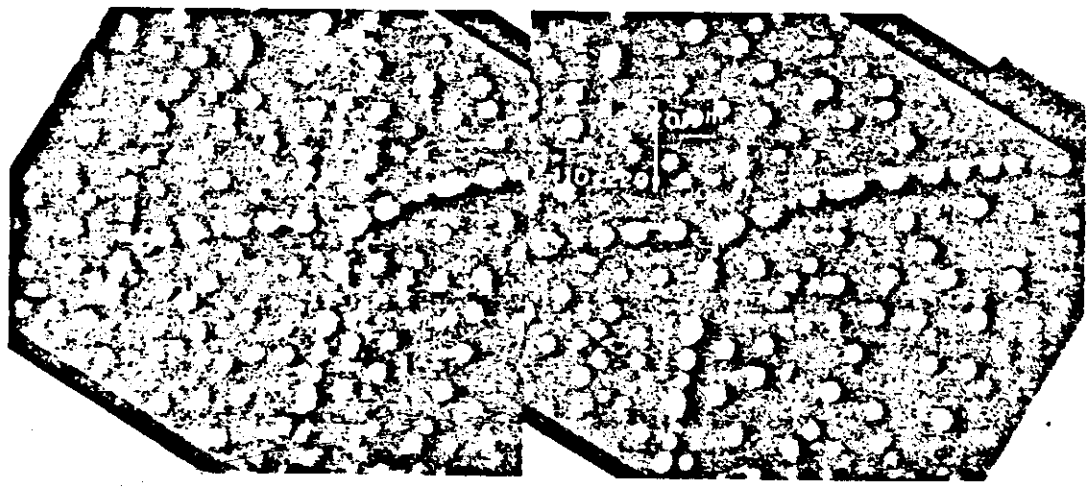

Fig. 6. Al–Li (2.2 wt%) aged at 230 C for 17 h. $\mathbf{g} = [110] + [220]$, stereo angle 24°.

Fig. 7. Al–Li (2.2 wt%) aged at 245 C for 115 h. Deformed till fracture. $\mathbf{g} = [00\bar{1}] + [02\bar{2}]$.

formed till fracture. In this case the microstructure as well as the NMR results look very different compared to those of Al–Li aged at 215 C (1 h). From stereo electron micrographs the average gap between the precipitates, L_p, is found to be 0.3 μm ($\bar{R} = 0.14\ \mu$m, $f = 5\%$). This value is close to the mean jump distance of 0.25 μm determined by NMR at low ϵ, indicating that in contrast to Al–Li aged at 215 C (1 h), Orowan hardening might be the predominant hardening mechanism. Figure 7 clearly shows that looping occurred during plastic deformation. The interparticle spacing in the slip direction sets an upper limit for the slip distance, i.e. the actual distance traversed before a dislocation gets stuck. The hardening is expected to be controlled by the microstructure at the beginning of deformation. At higher strain values the mean jump distance is decreasing gradually from 0.2 μm at $\epsilon = 5\%$ to 0.08 μm. The reason for this decrease is two-fold: first of all "statistically stored" dislocations, i.e. those that would accumulate during simple tension, will diminish the mean jump distance substantially. As can be deduced from Fig. 7 the mean distance between the statistically stored dislocations is certainly much smaller than the mean separation of the δ' precipitates. If moving dislocations are delayed at each intersection with the statistically stored dislocations during a period $\tau_r > 10^{-4}$ s, spin lattice relaxation takes place. As a result of the spin lattice relaxation $T_{1\rho}^{-1}$ is determined by waiting time at each intersection. The mean jump distance is therefore decreasing upon deformation from the mean particle spacing at the beginning of deformation to the spacing between statistically stored dislocations later on. Secondly, since it is unlikely that each precipitate is to be intersected by only one slip plane, loops are expected to form vertical stacks. Any movement of dislocation debris accumulated round these particles affect the spin lattice relaxation rate as well.

The experimental results obtained are in agreement with the stress strain equation given by Ashby's concept of "statistically stored" and "geometrically necessary" dislocations, i.e. those generated to accomplish the rotation of the non-deforming particles during deformation [16, 17], namely

$$\sigma \approx \mu b (\rho_G + \rho_u)^{1/2} \tag{10}$$

where the density ρ_G of geometrically necessary dislocations is given by

$$\rho_G \simeq \left(\frac{1}{\Lambda_G}\right)\frac{4\epsilon}{b}. \tag{11}$$

The geometric slip distance Λ_G is $\bar{R}/f$ (R, is the planar particle radius and f the volume fraction). Λ_G is considered to be characteristic of the microstructure and independent of the strain. The upper limit Λ_G in Al–Li containing nonshearable precipitates is calculated to be $\simeq 1\ \mu$m. Thompson *et al.* [18] proposed a modification to equation (10) where Λ_G sets an upper limit to Λ_u, the slip distance for a statistical storage, and $\Lambda_u \simeq \Lambda_G$ at yield. Then at small strain the slip distance is Λ_G and at large strain where $\Lambda_u \ll \Lambda_G$ it reduces to $\tau \sim \Lambda_u^{-1}$. This situation has been found in our experiments.

Figure 2 indicates that there exists a clear difference in functional dependence of L upon ϵ in these two Al–Li alloys. The mean jump distance is almost constant for $\epsilon \gtrsim 5\%$ in Al–Li containing shearable precipitates whereas L is still a decreasing function of ϵ in Al–Li containing nonshearable precipitates. These differences in behaviour are in agreement with the various workhardening rates. According to equation (2) the shear strain can be described by the mean jump distance L of the mobile dislocations according to $a = b\rho_m L$. In general, the flow stress can be expected to vary with dislocation density according to: $\tau = \alpha\mu b\sqrt{\rho}$. This gives the workhardening rate θ as

$$\frac{\delta\tau}{\delta a} = \frac{\alpha\mu\sqrt{b}}{2\sqrt{\rho}\left[\rho_m\left(\frac{dL}{d\rho}\right) + L\left(\frac{d\rho_m}{d\rho}\right)\right]}. \quad (12)$$

If L is assumed to be constant, θ becomes proportional to $1/L$ and ρ_m must increase with ρ according to $\rho_m \approx \sqrt{\rho}$. This is the situation for Al–Li containing shearable precipitates when $\epsilon \gtrsim 5\%$.

In contrast, since L is not constant up to $\epsilon = 15\%$ in Al–Li containing nonshearable precipitates

$$\frac{dL}{d\rho} \neq 0. \quad (13)$$

If L is not a constant, equation (12) can be rewritten in terms of the internal stress τ_i as (A is a constant)

$$\theta = \frac{A}{\tau_i\frac{dL}{d\tau_i} + L} \quad (14)$$

neglecting the thermal component of the flow stress which is much smaller than the athermal component in the case of f.c.c. metals. Since $(dL/d\rho)$ and $(dL/d\tau_i)$ are both negative ($L \approx \rho^{-1/2}$), the workhardening rate of Al–Li containing nonshearable precipitates is expected to be higher than θ of Al–Li containing shearable precipitates. Indeed, this is confirmed by the experimental σ–ϵ curves depicted in Fig. 8.

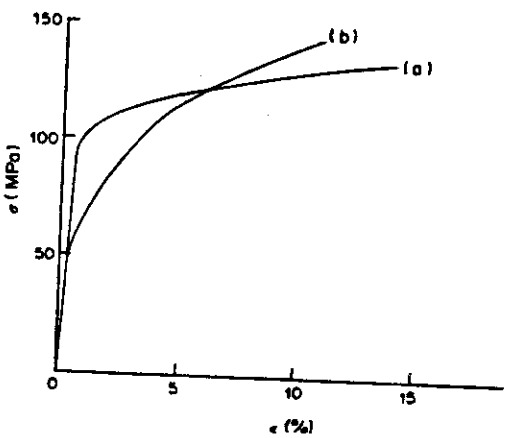

Fig. 8. Experimental stress–strain curve of *some* of the foils measured at 77 K. (a) Al–Li (2.2 wt%) aged at 215°C (1 h). (b) Al–Li (2.2 wt%) aged at 245°C (115 h).

The values of the mean jump distance obtained by NMR can be used for a theoretical evaluation of the yield stress. The yield stress of ultrapure Al at 77 K appeared to be equal to 10 MPa. Consequently, the increase of the yield stress of the samples aged at 215°C and aged at 245°C, compared to ultrapure Al, is 92 and 41 MPa, respectively (see Fig. 8). A calculation of the flow stress for a single dislocation, τ_i, taking into account the effective obstacle spacing as a function of applied stress for finite obstacles and slightly bent dislocations, has been given by Castagné [19]. The flow stress can be written as [13]

$$\tau_i = \frac{\gamma}{b}\left(\frac{2\bar{R}_s}{L_F}\right). \quad (15)$$

Dealing with superlattice dislocations, Brown and Ham [13] have shown that when the first dislocation of a superlattice dislocation pair meets the Friedel condition, the second dislocation is pulled forward by the anti phase boundary remaining in the particles which it intersects by τ_{APB} described by

$$\tau_{APB} = f\frac{\gamma}{b}. \quad (16)$$

The applied flow stress required for cutting the precipitates, τ_e, follows from

$$2\tau_e - \tau_i + \tau_{APB} = 0. \quad (17)$$

Taking the experimental values mentioned before (f, $\bar{R}$, γ) and $L_{NMR} \simeq L_F = 0.08\,\mu$m, τ_e is found to be 29 MPa. This is in close agreement with the increase of the applied yield stress ($\tau_e \simeq \sigma_e/3$) of Al–Li (aged at 215°C, 1 h) compared to ultrapure Al. As a matter of course, this increase should be compared with the as-quenched sample value. However, we could not obtain very reproducible results for those samples as far as the yield stress is concerned (12–28 MPa). Orowan looping will occur when $\tau_e = \frac{1}{2}\tau_0$. τ_0 [20, 21] is calculated to be 97 MPa. It means that as long as $\gamma_{APB} \leqslant 180$ mJ/m^2 shearing of the precipitates will take place.

In calculating the critical stress for looping in Al–Li aged at 245°C (115 h) the average gap between the precipitates is assumed to be $L_{NMR} \simeq 0.25\,\mu$m. τ_0 is calculated to be 31.4 MPa. Since the applied stress required for cutting [equation (17)] is much larger than $\tau_0/2$ the first dislocation within the superlattice dislocation pair reaches the looping stage. The connection between L_{NMR} and L_p, the average gap between the precipitates, will be discussed in Section 4.3.

4.2. *Activation length*

Mechanical tests involving a change in strain rate by a factor of ten were employed to measure $(\delta \ln \dot{\epsilon}/\delta\tau)_T$ [equation (5)], from which the apparent activation volume was deduced. The resulting data, depicted in Fig. 9, reveal that the apparent activation

volume and activation length for each alloy system decreases with increasing strain. This behaviour has been observed also in f.c.c. crystals using the same techniques, e.g. in Al by Mukherjee *et al.*, [22] and in Cu by Van Den Beukel and co-workers [23]. However, there exists a striking difference between the two Al–Li alloy systems with respect to the rate at which this decrease happens. This can be understood by the following arguments: the effective activation length represents the mean spacing of the forest dislocations [24]. As mentioned before in 4.1 in the Al–Li alloy containing shearable precipitates work-softening will take place [14], i.e. the slip will tend to be heterogeneous in such a material.

The tendency to produce heterogeneous slip will be more pronounced the more the flow stress resistance decrease by the passage of a dislocation. Once the δ' precipitates are sheared their resistance to further dislocation motion is reduced and strain localization will occur. It is obvious that under heterogeneous slip less rapid formation of stable dislocation configurations can arise as a result of reactions between the sets of slipping dislocations. The rate of strain hardening, based on the concept that the slipping dislocations interact to produce low energy configurations which then restrain motion of slipping dislocations, is expected to be small in the case of shearable δ' precipitates. This is in agreement with the experimental observations (Fig. 8). These findings are in contrast to the strain dependence of λ measured in Al–Li where Orowan loops are formed. In this material dislocation bypassing occurs and the workhardening of this slip plane leads to slip homogenization. On straining dislocation debris accumulates round the particles leading to workhardening of the slip plane upon which the dislocations have moved. It favours therefore the operation of a different slip plane, i.e. slip tends to become homogeneous. The workhardening is due to Orowan loops at low strains and to an increasing degree, due to prismatic loops at high strains [25, 26]. With increasing strain the number of prismatic loops increases, and therefore the length of the obstacles in slip plane increase, leading to a self-hardening of the slip line. At large strains even loops can be punched out on secondary systems (due to the back stress from the prismatic loops) and plastic zones of considerable complexity are formed leading to *forest hardening* [27]. Because these various hardening mechanisms are operative in Al+Li containing nonshearable precipitates, the activation length is expected to decrease with strainhardening more rapidly than in Al–Li containing shearable precipitates. Indeed, this is confirmed by the experimental observations depicted in Fig. 9. It should be noted that in the derivation of the activation length λ it was assumed that the obstacle width was independent of the applied stress and has the arbitrarily chosen value of b. In the Friedel approximation the effective activation length is proportional to the applied stress $\tau^{-1/3}$ [28]. This effective spacing is given approximately by

$$\lambda_F = \left(\frac{2T}{\tau b L_s}\right)^{1/3} L_s \tag{18}$$

where L_s is the mean square spacing [equation (8)]. (For shearable precipitates λ_F is actually identical to L_F. Substituting the mean square spacing [equation (8)] and $\tau = \tau_i$ [equation (15)] into equation (18) one arrives at equation (9)]. Based on equation (18) the activation volume will become equal to $2/3\ \lambda b^2$ leading to somewhat higher values of λ than depicted in Fig. 9.

4.3. Comparison between mean jump distance and activation length

In conclusion we may say that there exists mutual consistency between the main jump distance and the activation length as far as their effects on the hardening rates are concerned. However, there are considerable differences in magnitude between the activation length λ and the mean jump distance L in the two alloy systems. For instance, in the alloy (b) containing nonshearable precipitates $L_{NMR} > \lambda$ for $\epsilon > 5\%$ whereas in the alloy (a) containing shearable precipitates $L_{NMR} < \lambda$ over the whole range of deformation. In principle there is no physical reason why the mean activation length λ and mean jump distance L_{NMR} in these alloy systems should be identical. Precipitates, both shearable and nonshearable, cannot be passed by due to thermal fluctuations as in a strain rate-change experiment. Therefore, λ is determined by the forest dislocation density and Li impurities in solid solution. On the other hand, L_{NMR} depends on both the average gap between the precipitates and mean spacing between the forest dislocations. L is obtained from samples which are deformed with *constant*

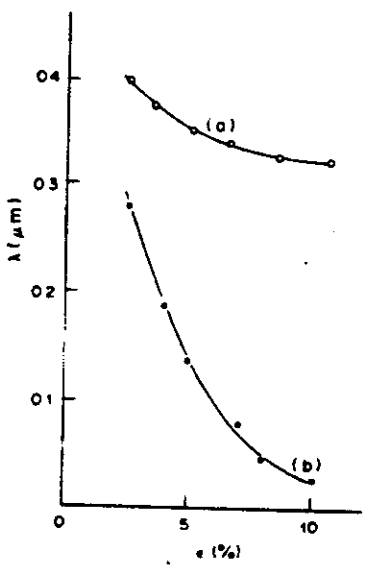

Fig. 9. Activated length determined from strain rate change experiments. The strain rate range is 10^{-6} to 10^{-1} s^{-1}. (a) Al–Li (2.2 wt%) aged at 215 C (1 h). (b) Al–Li (2.2 wt%) aged at 245 C (115 h).

strain rate $\dot{\epsilon}$ with increasing stress. This means that L is dynamically influenced by dislocation multiplication. The mean distance covered during a dislocation jump is controlled merely by relatively hard obstacles (precipitates, forest dislocations) since the effective stress is large enough to make the soft obstacles (Li in solid solution) contribute to the lattice friction only. *Changes in strain rate* during deformation, however, can cause similar effects to the flow stress as changes in temperatures. An increase in strain rate gives less time for thermally activated events: i.e. it is equivalent to a lowering of the temperature of deformation. As a consequence, hardening occurs because dislocations blocked by forest dislocations in the primary slip plane are not able to avoid them by cross slip. In addition, the cooperative way of dislocation dynamics will influence λ. A dislocation pinned at different obstacles may "unzip" along its entire length after thermal activation of only one segment of the dislocation across one barrier, since at that very moment the critical breakaway angle of all other segments is exceeded. Only a small activation volume V per segment would be measured and consequently a small λ, although L_{NMR} in that case need not be influenced by this unzipping effect.

A plausible connection between λ and L_{NMR} can be based on the following model: all moving dislocations, delayed at intersections with either forest dislocations or precipitates, affect the spin-lattice relaxation rate. Assuming two different sets of corresponding mobile dislocation densities: ρ_1 and ρ_2, respectively, the total spin lattice relaxation rate can be written as

$$\left(\frac{1}{T_{1\rho}}\right)_D = \left(\frac{1}{T_{1\rho}}\right)_D^{(1)} + \left(\frac{1}{T_{1\rho}}\right)_D^{(2)} \tag{19}$$

where [see equation (3)]

$$\left(\frac{1}{T_{1\rho}}\right)_D^{(1)} \approx \frac{\rho_1}{L_1\rho} \quad \text{and} \quad \left(\frac{1}{T_{1\rho}}\right)_D^{(2)} \approx \frac{\rho_2}{L_2\rho} \tag{20}$$

and $\rho_1 + \rho_2 = \rho$. L_1 represents the spacing between forest dislocations, λ, and L_2 is the gap between the precipitates, L_p. In equation (19) the contribution to the spin-lattice relaxation rate due to any movement of dislocation debris accumulated round the precipitates has been neglected. At $\epsilon = 5\%$ alloy (b), λ is found to be 0.14 μm and the average gap between the nonshearable precipitates $L_p = 0.3\,\mu$m. Assuming equal fractions ($\rho_1 = \rho_2$), the mean jump distance L_{NMR} is calculated to be 0.19 μm, according to

$$\frac{1}{L_{NMR}} \simeq \frac{\rho_1}{\lambda\rho} + \frac{\rho_2}{L_p\rho}. \tag{21}$$

This is almost equal to the experimentally determined value (Fig. 2). From equation (21) follows that, providing $\rho_1 \neq 0$, L_{NMR} is always smaller than the gap between the precipitates L_p (= constant). Assuming equal fractions ($\rho_1 = \rho_2$) up to $\epsilon = 10\%$, L_{NMR} is predicted to be 0.07 μm ($\lambda = 0.04\,\mu$m, $L_p = 0.3\mu$m). Again, this is in agreement with experiments (Fig. 2). Based on the experimental values of λ and L_p, L_{NMR} should be larger than λ in the alloy containing nonshearable precipitates.

An Al–Li containing shearable precipitates (alloy a) the relationship between L_{NMR} and λ is more complicated. In this case L_{NMR} and λ are almost constant over the whole range of deformation. On the contrary, L_p depends on ϵ since the cross section of the precipitate in the slip-plane will be reduced upon deformation. Further, it is likely that moving dislocations inside the precipitates contribute to the spin-lattice relaxation rate separately. When a mobile dislocation crosses over a distance L_p and subsequently short jumps occur over a distance $\bar{d}$, the mean diameter of the precipitates, the total spin lattice relaxation rate measured by NMR is largely determined by the jump distance inside the precipitates: ($\bar{d} < L_p \ll \lambda$)

$$\frac{1}{L_{NMR}} \simeq \frac{\rho_1}{\lambda\rho} + \frac{\rho_2}{L_p\rho} + \frac{\rho_3}{\bar{d}\rho} \tag{22}$$

apparently leading to $L_{NMR} < \lambda$.

5. CONCLUSIONS

It turned out that pulsed nuclear magnetic resonance is a complementary new technique for the study of moving dislocations in Al–Li alloys. Spin-lattice relaxation measurements clearly indicated that the fluctuations in the quadrupolar field due to moving dislocations in alloys containing either shearable or nonshearable precipitates are quite different. The NMR experiments provided information of the mean jump distance of dislocations in these alloys. Transmission electronmicroscopic observations of the mean planar diameter of the precipitates, in combination with the NMR data, predicted the increase of the yield stress compared to ultrapure aluminium in reasonable agreement with experiment. It was found that the activation length, obtained from mechanical strain rate change experiments, have different values compared to the measured values of the mean jump distance determined by NMR. Reasons for the mean jump distance being different from activation length have been given. Nevertheless, both mean jump distance and activation length have been found to decrease with strain hardening more rapidly in Al–Li containing nonshearable precipitates than in Al–Li containing shearable precipitates. These findings are consistent with the experimentally measured workhardening rates.

Finally, it should be emphasized that Al–Li alloy is not an alloy system that exhibits only one type of hardening: i.e. order hardening or Orowan hardening. Plastic deformation is a local process and as a consequence depends on the local characteristics of the microstructure. Since there exists a distribution of particle sizes both hardening mechanisms may occur. Nonetheless, NMR measurements clearly showed different fluctuations in the local magnetic field due

to moving dislocations in these two alloys from which a difference in dislocation dynamics may be concluded.

Acknowledgements—The authors should like to thank Professor A. Van Den Beukel for valuable discussion and for critical reading of the manuscript. Thanks are due to Dr L. Katgerman (Technological University, Delft), providing us with the raw Al–Li material. We thank Mr U. Schlagowski for the technical assistance in the NMR measurements. The work is part of the research program of the Foundation for Fundamental Research on Matter (F. O. M., Utrecht) and has been made possible by financial support from the Netherlands Organization for the Advancement of Pure Research (Z. W. O., The Hague) and the Deutsche Forschungsgemeinschat, F.R.G.

REFERENCES

1. *Proc. Conf. Aluminium–Lithium Alloys* (edited by T. N. Sanders and E. A. Starke), Am. Inst. Min. Engrs, New York (1981).
2. T. H. Sanders and E. A. Starke, *Acta metall.* **30**, 927 (1982).
3. J. Th. M. De Hosson, O. Kanert, A. W. Sleeswyk, in *Dislocations in Solids* (edited by F. R. N. Nabarro). Vol. 6, Chap. 32, pp. 441–534. North-Holland, Amsterdam (1983).
4. H. Tamler, O. Kanert, W. H. M. Alsem and J. Th. M. De Hosson, *Acta metall.* **30**, 1523 (1982).
5. H. J. Hackelöer, O. Kanert, H. Tamler and J. Th. M. De Hosson, *Rev. scient. Instrum.* **54**, 341 (1983).
6. J. Th. M. De Hosson, W. H. M. Alsem, H. Tamler and O. Kanert, in *Defects, Fracture and Fatigue* (edited by G. C. Sih and J. W. Provan), p. 23. Nijhoff, The Netherlands (1982).
7. E. Orowan, *Z. Phys.* **89**, 634 (1934).
8. U. F. Kocks, A. S. Argon and M. F. Ashby, in *Progress in Materials Science* (edited by B. Chalmers, J. W. Christian and T. B. Massalski), Vol. 19, p. 1. Pergamon Press, Oxford (1975).
9. J. Th. M. De Hosson, O. Kanert and H. Tamler, in *Aluminium–Lithium Alloys* (edited by T. H. Sanders and E. A. Starke). Am. Inst. Min. Engrs, New York (1983).
10. O. Kanert and M. Mehring, *Static Quadrupole Effects in Disordered Cubic Solids, NMR*, Vol. 3. Springer, Berlin (1971).
11. U. F. Kocks, in *Fundamental Aspects of Dislocation Theory* (edited by J. A. Simmons, R. De Wit and R. Bullough), Vol. 2, p. 1077. NBS Spec. Publ. 317. (1970).
12. D. J. H. Cockayne, *Z. Naturf.* **27a**, 452 (1972).
13. L. M. Brown and R. K. Ham, in *Strengthening Methods in Crystals* (edited by A. Kelly and R. B. Nicholson), p. 12. Appl. Sci. Publ., London (1971).
14. J. W. Martin, *Micromechanisms in Particle-Hardened Alloy*. Cambr. Solid St. Sci. Ser., Cambridge (1980).
15. M. Tamura, T. Mori and T. Nakamura, *Trans. Japan Inst. Metals* **14**, 355 (1973).
16. M. F. Ashby, *Phil. Mag.* **21**, 399 (1970).
17. K. C. Russell and M. F. Ashby, *Acta metall.* **18**, 891 (1970).
18. A. W. Thompson, M. I. Baskes and W. F. Flanagan, *Acta metall.* **25**, 1017 (1973).
19. J. L. Castagné, *J. Physique* **27**, C3-233 (1966).
20. P. B. Hirsch and F. J. Humphreys, *The Physics of Strength and Plasticity* (edited by A. S. Argon). M.I.T. Press, MA (1969).
21. P. M. Kelly, *Int. Metall. Rev.* **18**, 31 (1973).
22. A. K. Mukherjee, J. D. Mote and J. E. Dorn, *Trans. metall. Soc. A.I.M.E.* **233**, 1559 (1965).
23. G. Den Otter, Thesis, Technological University Delft, (1978); G. Den Otter and A. Van Den Beukel, *Physica status solidi* (a) **55**, 785 (1979).
24. A Seeger, *Dislocation and Mechanical Properties of Crystals*, pp. 243–332. Wiley, New York (1956).
25. P. B. Hirsch, in *The Physics of Metals*, Vol. 2, p. 189. Cambridge Univ. Press (1975).
26. P. B. Hirsch and F. J. Humphreys, *Proc. R. Soc.* **A318**, 45 (1970).
27. M. F. Ashby, *Strengthening Methods in Crystals* (edited by A. Kelly and R. B. Nicholson), p. 137. APPL. Sci., London (1971).
28. J. Friedel, *Dislocations*. Pergamon Press, New York (1964).

(2)

Reprinted from

ACTA METALLURGICA

Vol. 34, *No.* 8, *pp.* 1571–1581

SOLUTION HARDENING IN Al–Zn ALLOYS. MEAN JUMP DISTANCE AND ACTIVATION LENGTH OF MOVING DISLOCATIONS

J. TH. M. DE HOSSON and G. BOOM

Department of Applied Physics, Materials Science Centre, University of Groningen, Nijenborgh 18, 9747 AG Groningen, The Netherlands

U. SCHLAGOWSKI and O. KANERT

Institute of Physics, University of Dortmund, 4600 Dortmund 50, F.R.G.

PERGAMON PRESS
OXFORD · NEW YORK · BEIJING · FRANKFURT
SÃO PAULO · SYDNEY · TOKYO · TORONTO
1986

Acta metall. Vol. 34, No. 8, pp. 1571–1581, 1986
Printed in Great Britain

0001-6160/86 $3.00 + 0.00
Pergamon Journals Ltd

SOLUTION HARDENING IN Al–Zn ALLOYS

MEAN JUMP DISTANCE AND ACTIVATION LENGTH OF MOVING DISLOCATIONS

J. TH. M. DE HOSSON and G. BOOM
Department of Applied Physics, Materials Science Centre, University of Groningen, Nijenborgh 18, 9747 AG Groningen, The Netherlands

and

U. SCHLAGOWSKI and O. KANERT
Institute of Physics, University of Dortmund, 4600 Dortmund 50, F.R.G.

(*Received* 25 *July* 1985; *in revised form* 10 *December* 1985)

Abstract—Pulsed nuclear magnetic resonance proved to be a complementary new technique for the study of moving dislocations in Al–Zn alloys. The NMR technique, in combination with strain-rate change experiments and transmission electron microscopy have been applied to study dislocation dynamics in Al–Zn alloys (1–2 at.% Zn). Spin-lattice relaxation measurements clearly indicate that fluctuations in the quadrupolar field caused by moving dislocations in Al–Zn are different compared to those in ultra-pure Al. From the motion induced part of the spin-lattice relaxation rate the mean jump distance of mobile dislocations has been measured as a function of strain. Based on the NMR data and data obtained from strain-rate change experiments it could be concluded that moving dislocations advance over a number of solute atoms (order of 10) as described by Mott–Nabarro's model and interact with forest dislocations as predicted by Friedel's model. The strain rate change experiments confirm the linear additivity of flow stresses and the additivity of inverse activation length.

Résumé—La résonance magnétique nucléaire pulsée est une nouvelle technique complémentaire pour l'étude des dislocations en cours de déplacement dans des alliages Al–Zn. Nous avons appliqué la RMN, combinée avec des expériences de sauts de la vitesse de déformation et avec la microscopie électronique en transmission pour étudier la dynamique des dislocations dans des alliages Al–Zn (1–2 at.% Zn). Des mesures de relaxation spin-réseau montrent clairement que les fluctuations dans le champ quadrupolaire provoquées par les dislocations en mouvement dans Al–Zn sont différentes de celles que l'on observe dans l'aluminium ultrapur. A partir de la partie de la vitesse de relaxation spin-réseau induite par le mouvement des dislocations, nous avons mesuré la distance moyenne de saut des dislocations mobiles en fonction de la déformation. A partir des résultats de RMN et des expériences de changement de la vitesse de déformation, nous avons pu conclure que les dislocations en cours de déplacement avancent d'un certain nombre d'atomes de soluté (de l'ordre de 10) suivant le modèle de Mott et Nabarro et que'elles interagissent avec les dislocations de la forêt comme le modèle de Friedel le prévoit. Les expériences de saut de vitesse de déformation confirment l'additivité linéaire des contraintes d'écoulement et l'additivité de l'inverse de la longueur d'activation.

Zusammenfassung—Gepulste Kernspinresonanz hat sich als eine neue ergänzende Methode zur Untersuchung der Bewegung von Versetzungen in Al–Zn-Legierung bewährt. Diese Technik wurde zusammen mit Untersuchungen durch Dehngeschwindigkeitswechsel und im Durchstrahlungselektronenmikroskop auf die Untersuchung der Versetzungsdynamik in Al–Zn-Legierungen (1–2 At.-% Zn) angewendet. Messungen der Spin-Gitter-Relaxation zeigen deutlich, daß die von den gleitenden Versetzungen erzeugten Fluktuationen im Quadrupolfeld sich in Al–Zn von denen im ultrareinen Al unterscheiden. Aus dem Bewegungs-induzierten Teil der Spin-Gitter-Relaxationsrate kann die mittlere Sprungweite einer beweglichen Versetzung in Abhängigkeit von der Dehnung ermittelt werden. Aus den Kernspinresonanz- und Dehngeschwindigkeitswechsel-Messungen konnte geschlossen werden, daß die gleitenden Versetzungen sich über eine Anzahl gelöster Atome (Größenordnung von 10) hinweg bewegen, wie es im Modell von Mott und Nabarro beschrieben ist, und mit Waldversetzungen wechselwirken, wie vom Modell von Friedel vorausgesagt. Die Experimente mit Dehngeschwindigkeitswechseln bestätigen die lineare Additivität der Fließspannungen und die Additivität der inversen Aktivierungslängen.

1. INTRODUCTION

Magnetic resonance spectroscopy ranks among one of the important advances in solid state physics during the past three decades. The great strength of nuclear magnetic resonance is that the resonance signal is characteristic of a particular nucleus being studied. Because the nuclei of many elements are characterized by intrinsic magnetic moments, the resonance frequency ω_0, in a magnetic field H_0, equals γH_0, where the gyromagnetic ratio γ is a constant which is different for different nuclei. As a result, nuclear magnetic resonance (NMR) can be

used to measure properties which belong exclusively to the nuclei whose features are of interest. Secondly, the surrounding of a nucleus may affect NMR quantities like spin-lattice relaxation time. Accordingly, NMR can be applied to study the environment of the nuclei providing microscopic information of atomic motions. In the following, we report effects of dislocation motion in Al–Zn alloys on the NMR spin-lattice relaxation time, from which microscopic information about the dislocation dynamics can be obtained. Whenever a dislocation changes its position in the crystal, the surrounding atoms have also to move, thus causing time fluctuations of the quadrupolar field that dominates the observed spin-lattice relaxation behaviour.

In the following we will focus mainly on plastic deformation experiments at a constant strain rate $\dot{\epsilon}$. This type of experiment is governed by Orowan's equation [1]

$$\dot{\epsilon} = \phi b \rho_m \frac{L}{\tau_m} \tag{1}$$

assuming a jerky motion of mobile dislocations of density ρ_m. This motion may be considered to be jerky, if the actual jump time τ_j is small compared to the mean time of stay τ_m at an obstacle. In equation (1), ϕ denotes a geometrical factor, b symbolizes the magnitude of the Burgers vector and L is the mean jump distance between obstacles which are considered to be uniform. Clearly, alloying introduces extra barriers to the motion of dislocations. Therefore, during plastic deformation of a binary solid solution such as Al–(1–2 at.%)Zn, moving dislocations are hindered in their glide plane by two types of obstacles: forest dislocations and solute atoms. The theory of obstacle strengthening can be complicated and Nabarro [2,3] has shown how the important features can be distinguished. Nevertheless, it has been recognized from the time of the earliest theories that it is difficult to estimate the segment length of a dislocation line that advances *during* plastic flow. NMR techniques can provide experimental information about the length of a moving dislocation line segment. The NMR results obtained are compared with the average obstacle spacing determined by mechanical strain rate change experiments.

2. THEORETICAL BACKGROUND

The NMR method of obtaining microscopic information about moving dislocations is essentially based on the interaction between nuclear electric quadrupole moments and electric field gradients at the nucleus. If the nuclear environment is cubically symmetric there does not exist any static electric field gradient at the nucleus and the interaction does not appear. However, around a dislocation that symmetry is destroyed and interactions between nuclear electric quadrupole moments and electric field gradients arise. When the condition of non-vanishing electric field gradients is fulfilled, spin-lattice relaxation times are influenced by the quadrupole interaction. Whenever a dislocation changes its position in the crystal, the surrounding atoms have also to move, causing time fluctuations in this quadrupolar Hamiltonian. Further, for the investigation of rather infrequent defect motions as in the case of moving dislocations, the spin-lattice relaxation time in the rotating frame, $T_{1\rho}$, has proved to be the most appropriate NMR quantity affected by such motions. For detailed information of this technique reference is made to previous work [4–7]. Only a concise review will be presented here.

While deforming a sample at a constant strain rate $\dot{\epsilon}$, the spin-lattice relaxation rate in a weak rotating field H_1, $T_{1\rho}^{-1}$, of the resonant nuclei in the sample is enhanced due to the motion of dislocations. The resulting total relaxation rate may be decomposed into a background relaxation rate $(T_{1\rho}^{-1})_0$ and the contribution $(T_{1\rho}^{-1})_D$ which is governed by the mechanism of dislocation motion, i.e. by equation (1). In metals and alloys $(T_{1\rho}^{-1})_0$ is due to fluctuations in the conduction electron–nucleus interaction. In the range of deformation rates applied here the atomic movements involved in dislocation motion are in the so-called ultra-slow motion region, where the Zeeman spin-lattice relaxation rate T_1^{-1} and the spin-spin relaxation rate T_2^{-1} are not markedly influenced by dislocation motion and where the rotating frame relaxation rate $(T_{1\rho}^{-1})$ is the most appropriate NMR parameter affected by such motion. The resulting expression for the relaxation rate induced by dislocation motion is given by [4]

$$\left(\frac{1}{T_{1\rho}}\right)_D = \frac{A_Q}{H_1^2 + H_{loc}^2} g_Q(L) \frac{\rho_m}{\tau_m} \tag{2}$$

where $A_Q = \delta_Q \langle V^2 \rangle$. δ_Q represents a quadrupolar coupling constant, depending on the nuclear quadrupole moment Q, on the nuclear spin I and on the gyromagnetic ratio γ, and $\langle V^2 \rangle$ denotes the second moment of the electric field gradient due to the stress field of a dislocation of unit length. The value of A_Q can either be determined theoretically or derived experimentally [4, 8]. H_{loc} is the mean local field in the rotating frame determined by the local quadrupolar field H_Q and the local dipolar field H_D. The quadrupolar geometry factor $g_Q(L)$ in equation (2) which depends on the mean step width L is displayed in Fig. 1, where the jump distance L is expressed in units of b: $N = L/b$.

Typically, in plastic deformation experiments the jump distance L is of the order of 0.1–1 μm, i.e. N is of the order of 10^3. For such large jump distances, $g_Q(L)$ approaches to unity being not very sensitive to a change in L.

It has to be noted that equation (2) is valid only in the so-called "strong-collision" region where the dislocation motion is slow enough to allow the spins to establish a common spin-temperature between suc-

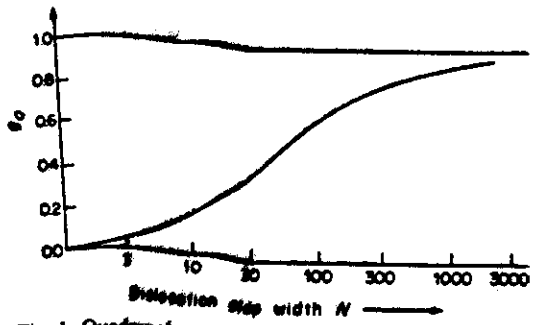

Fig. 1. Quadrupolar geometry factor g_Q of a mobile dislocation as a function of the normalized jump distance N (in units of the Burgers vector).

cessive dislocation jumps. In practice, the condition is fulfilled for strain-rates up to $10\,s^{-1}$ depending slightly on $H_1^2 + H_{\text{loc}}^2$. If only a few discrete jumps of an atom caused by dislocation motion are needed to relax a spin, the "collisions" are called "strong". More precisely, the spin part of the corresponding correlation function of the jerky atomic motion decays before the geometrical part of the correlation function changes considerably. Combining equation (1) with equation (2) one obtains

$$\left(\frac{1}{T_{1\rho}}\right)_D = \frac{\phi}{H_1^2 + H_{\text{loc}}^2} \frac{1}{\phi b} \frac{g_Q(L)}{L} \dot{\epsilon}. \qquad (3)$$

Hence, for a given shear strain rate $\dot{\epsilon}$ the dislocation induced spin-lattice relaxation rate is proportional to the inverse of the mean jump distance L. This relationship is used in the experiments discussed below to determine $\dot{\epsilon}$.

On the other hand the shear strain rate can be written as [9]

$$\dot{\epsilon} = \dot{\epsilon}_0 \exp\left(-\frac{\Delta G}{kT}\right) \qquad (4)$$

where ΔG is the activation energy for intersection, being the only release of a dislocation from an obstacle is due to thermal fluctuations. Arrhenius' type of behaviour of $\dot{\epsilon}$ holds for the flow stress [10]. The apparent activation volume is defined as

$$V = -\left(\frac{\delta \Delta G}{\delta \tau}\right)_T = kT\left(\frac{\delta \ln \dot{\epsilon}}{\delta \tau}\right)_T \simeq \lambda b^2 \qquad (5)$$

where λ is independent of the shear stress τ. λ represents the average obstacle spacing or the activated length. In the derivation of λ [equation (5)] it is assumed that the obstacle width is independent of τ and has the chosen value of b. Further derivation of the activated length with respect to τ is taken into account in equation (5). Creep tests involving a change in strain rate by a factor of ten have been employed to measure $(\delta \ln \dot{\epsilon}/\delta \tau)_T$ from which the average λ value has been deduced.

3. EXPERIMENTAL

In the NMR experiments, the sample under investigation is plastically deformed by a servo-hydraulic tensile machine (Zonic Technical Lab. Inc., Cincinnati) of which the exciter head XCI-TE 1105 moves a driving rod with a constant velocity. While the specimen is deforming, ^{27}Al nuclear spin measurements are carried out by means of a Bruker pulse spectrometer SXP-4-100 operating at 15.7 MHz corresponding to a magnetic field of 1.4 T controlled by an NMR stabilizer (Bruker B-SN 15). The NMR head of the spectrometer and the frame in which the rod moves formed a unit which was inserted between the pole pieces of the electromagnet of the spectrometer. A scheme of the experimental set-up is displayed in Fig. 2. As shown in the block diagram, the spectrometer is triggered by the electronic control of the tensile machine. The trigger starts the nuclear spin relaxation experiment at a definite time during the deformation determined by the delay time of the trigger pulse. Immediately before and after the plastic deformation the magnitude of the background relaxation rate $(T_{1\rho}^{-1})_0$ is measured.

From the experimental $T_{1\rho}$-data, the dislocation induced contribution of the relaxation time $(T_{1\rho})_D$ can be determined according to

$$\left(\frac{1}{T_{1\rho}}\right)_D = \left(\frac{1}{T_{1\rho}}\right)_{\text{tot}} - \left(\frac{1}{T_{1\rho}}\right)_0. \qquad (6)$$

A typical result of an *in situ* NMR tensile experiment on ^{27}Al is depicted in Fig. 3. A $\pi/2$ pulse with an r.f. field large compared to the local fields in the Al-sample along the x-direction rotates the nuclear magnetization from the direction of the static magnetic field to the y-direction. Immediately after the pulse, the r.f. field is phase shifted by $\pi/2$ and reduced to a value of H_1. Now H_1 lies parallel to the direction of the nuclear magnetization; with respect to the rotating frame, H_1 plays the role of a time-independent field. Consequently, the rotating magnetization relaxes parallel to the locking field H_1 with a time constant $T_{1\rho}$, i.e. the relaxation time in the rotating frame. To measure $T_{1\rho}$, the nuclear magnetization is allowed to decrease in the presence of the locking field H_1 for some time τ_L, then H_1 is turned off and the initial *height* of the nuclear free induction decay signal $F(\tau_L)$ is measured.

According to Fig. 3

$$\left(\frac{1}{T_{1\rho}}\right)_D = \frac{1}{\tau_L} \ln \frac{F(\tau_L)\dot{\epsilon} = 0}{F(\tau_L)\dot{\epsilon} \neq 0}. \qquad (7)$$

Obviously an applied strain rate $\dot{\epsilon}$ causes a significant reduction in the relaxation time $T_{1\rho}$ due to the motion of dislocations. An evaluation of the experiment leads to $T_{1\rho}\,(\dot{\epsilon} = 0) = 25$ ms and $T_{1\rho}\,(\dot{\epsilon} = 3.6\,s^{-1}) = 7.2$ ms, respectively.

To avoid skin effect distortion of the NMR signal, the NMR experiments are carried out on rectangular foils of size 27 mm × 12 mm × 40 μm. Polycrystalline

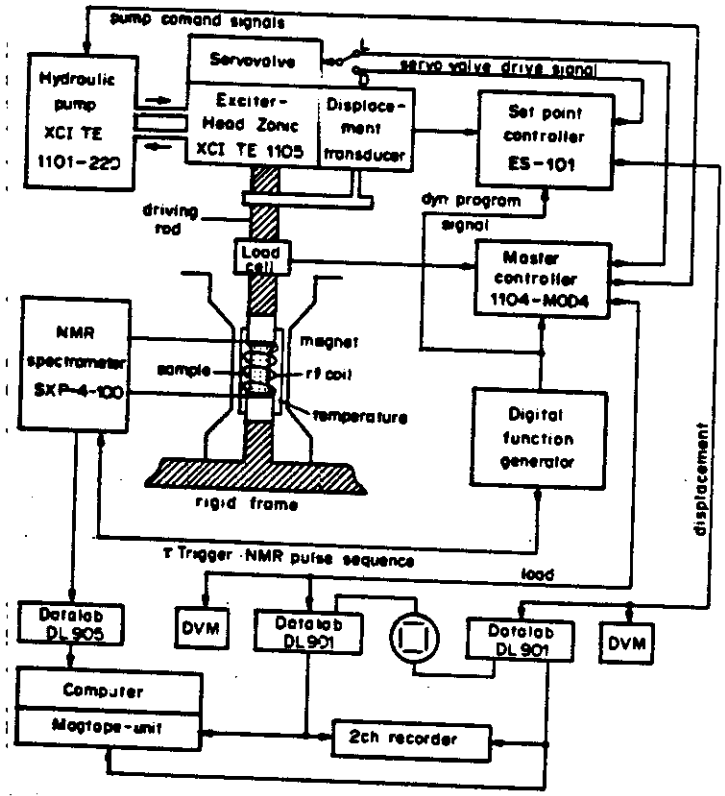

Fig. 2. Blockdiagram of the experimental set-up.

samples with a grain size in the order of 100–200 μm were used. The starting materials for the samples are (a) 5N aluminium and (b) 5N Al:1, 1.5, 2 at.% Zn. After homogenizing procedures at 550°C for 2.5 days, the material is rolled to thin foils with a thickness of about 40 μm and is cut by spark erosion to the sample size given above. Then the samples (a) consisting of ultrapure Al are annealed a second time at 290°C for 1 h. The Al–Zn alloys are annealed at 550°C for 1 h and quenched in ice water.

The NMR experiments discussed here are carried out at $T = 77$ K. At such a low temperature nuclear

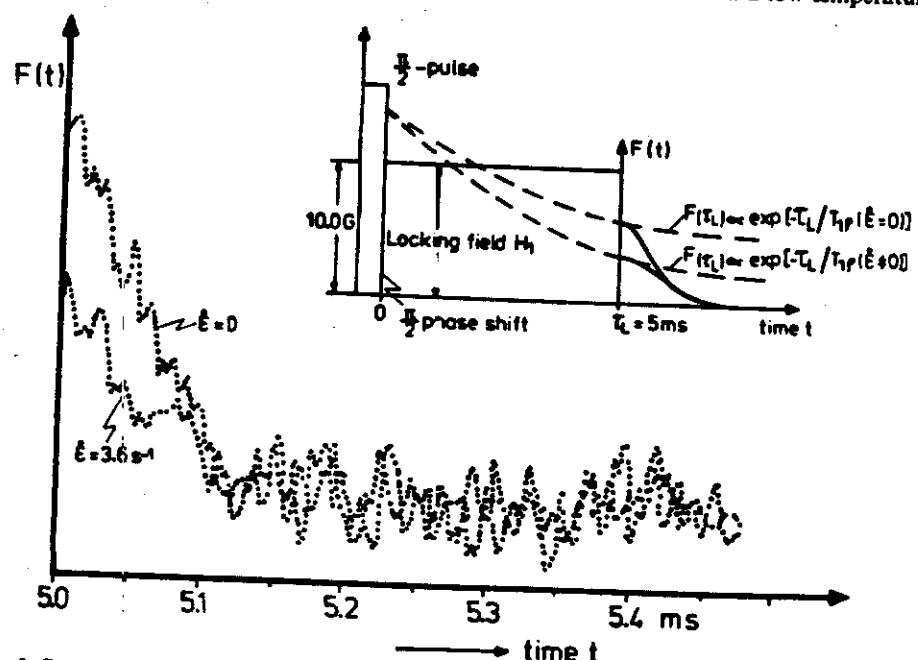

Fig. 3. Result of an *in situ* NMR tensile experiment showing the ^{27}Al free induction decays $F(t)$ in Al after a spin-locking sequence with $\dot{\varepsilon} = 0$ and $\dot{\varepsilon} \neq 0$. ($T = 77$ K).

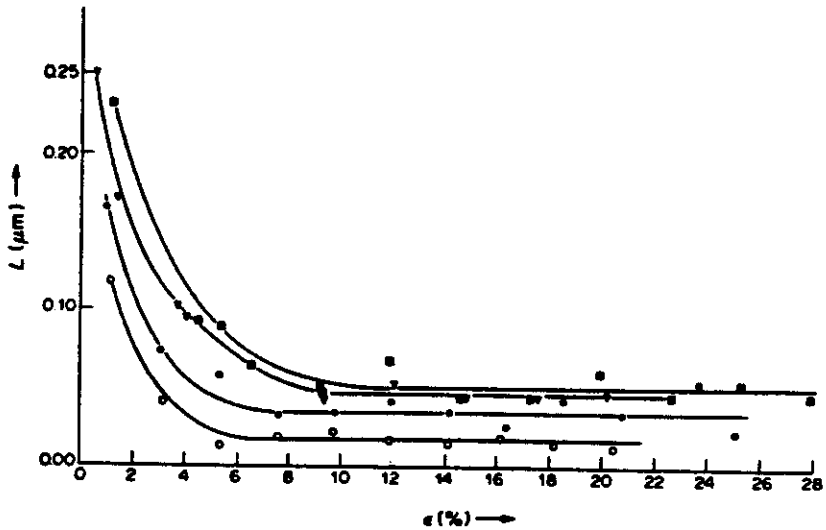

Fig. 4. Mean jump distance measured by NMR as a function of strain in: ■, Al; ▼, Al–1 at.% Zn; ●, Al–1.5 at.% Zn; ○, Al–2 at.% Zn ($\dot{\epsilon} = 1.6\,s^{-1}$).

spin relaxation effects because of diffusive atomic motions are negligible. The self-diffusion coefficient as well as the impurity diffusion of Zn in aluminum are published in the literature [11, 12]. Use of these data in the Einstein–Smoluchowski relation (connecting the diffusion coefficient D with the mean time of stay of an atom between two diffusion jumps), proves that Al and Zn atoms are actually immobile at 77 K. The correlation times for diffusive atomic jumps are much longer than typical values of the waiting time of mobile dislocations, which are about 10^{-4} s for $\dot{\epsilon} \simeq 1\,s^{-1}$. Consequently, an observable contribution of diffusive atomic motions to the measured spin-lattice relaxation rate does not occur.

Transmission electron micrographs are taken by using a JEM 200 CX. Disk-type specimens are obtained from the deformed foils by spark cutting to minimize deformation. The samples are electrochemically thinned in a polishing equipment at room temperature in a solution of 49% methanol, 49% nitric acid and 2% hydrochloric acid.

4. RESULTS AND DISCUSSION

4.1. Mean jump distance

The strain dependence of L has been obtained from measuring $(T_{1\rho}^{-1})$ as a function of the strain ϵ. The results of ultrapure Al and the various Al–Zn alloys are depicted in Fig. 4, taking into account the geometrical factor $g_0(L)$ displayed in Fig. 1. It has to be emphasized that the mean jump distance L measured by NMR in pure Al has to be interpreted with care in terms of the mean slip distance and the statistical slip length (Λ_{st}). As commonly found in annealed f.c.c. metals, a cell structure is developed in Al after deformation at 77 K. A stereo TEM-observation is shown in Fig. 5. As a result, the mean slip distance of dislocations is mainly determined by the cell size when the cell structure is well developed. Consequently, the slip length will be much larger than the mean jump distance measured by NMR ($\sim 0.05\,\mu$m for $\epsilon > 10\%$). To explain this difference, it has to be realized that *all* moving dislocations, present both in the cell boundary and in the interior region of the cell, affect the spin-lattice relaxation rate. Assuming two different sets of corresponding mobile dislocation densities, ρ_1 in the interior of the cell and ρ_2 inside the cell wall, the total spin-lattice relaxation rate can be decomposed in

$$\left(\frac{1}{T_{1\rho}}\right)_D = \left(\frac{1}{T_{1\rho}}\right)_D^{(1)} + \left(\frac{1}{T_{1\rho}}\right)_D^{(2)} \tag{8}$$

where

$$\left(\frac{1}{T_{1\rho}}\right)_D^{(1)} \sim \frac{\rho_1}{L_1\rho} \quad \text{and} \quad \left(\frac{1}{T_{1\rho}}\right)_D^{(2)} \sim \frac{\rho_2}{L_2\rho}$$

and $\rho_1 + \rho_2 = \rho_m$. Since $L_1 \gg L_2$, the total spin lattice relaxation rate is largely determined by the jump distance L_2 inside the cell wall. The mean jump distance measured by NMR at large strain values is therefore related to the spacing of the forest dislocation tangles in the cell boundary.

To investigate whether the observed mean jump distance has the right order of magnitude, we consider forest dislocations as relatively weak localized obstacles for dislocation motion, i.e. the dislocation bends through a large angle ϕ_c in its vicinity (ϕ_c: the cusp angle at an obstacle or the so-called critical breaking angle). Assuming Friedel statistics [9], the effective obstacle spacing λ_e can be related to the average inter-obstacle spacing λ according to

$$\lambda_e = \frac{\lambda}{\sqrt{f_1}} = \left(\frac{\mu b}{\tau_1 \lambda}\right)^{1/3} \lambda \tag{9}$$

where f_1 is a measure of the obstacle strength ($= \cos 1/2\,\phi_c$). On the other hand the effective flow

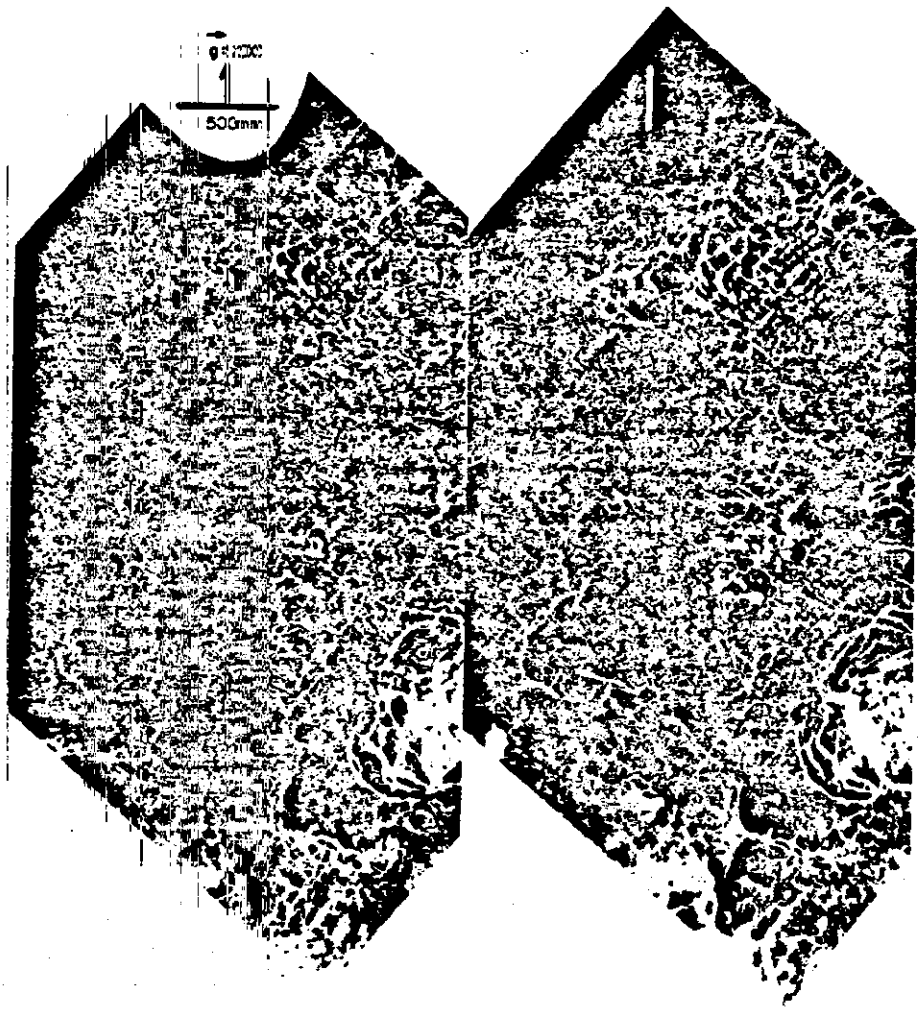

Fig. 5. Stereo-electron micrograph of ultrapure Al deformed at 77 K until fracture. g = 200, stereo angle 14.6°, stereo impression [013].

stress can be written as

$$\tau_i = \alpha \mu b \sqrt{\rho_F} \tag{10}$$

i.e. the applied stress is diminished by the athermal forest resistance and the interplane resistance. Although there exists some discussion about equation (10) whether the flow stress is controlled by intersection between primaries and forest dislocation density ρ_F, experimental work suggests that the flow stress in pure f.c.c. in stage II is controlled by forest dislocations or that forest contributions are always in a constant ratio independent of the dislocation distribution [13]. The estimated value of α for aluminium is about 0.1 [14] assuming that the flow stress is fully controlled by dislocation intersection with forest dislocations. From equations (9) and (10) follows $f_1 = \alpha^{2/3} = 0.21$ taking $\lambda \simeq \rho_F^{-1/2}$. On average the flow stress was found to increase from the flow stress at $\epsilon = 1\%$ of 14.6 MPa to 33 MPa at $\epsilon = 10\%$. The effective obstacle spacing λ_e [equations (9), (10)] is predicted to be proportional to τ_i^{-1}. Hence, λ_e is expected to decrease by a factor of 7. Indeed, this is in reasonable agreement with the NMR measurements: at the beginning of deformation L_{NMR} is found to be 0.25 μm decreasing to 0.05 μm at $\epsilon = 10\%$.

In Fig. 4 L measured by NMR in the Al–Zn alloys is illustrated as a function of strain. The shape of the L vs ϵ curve is quite similar to the curve obtained for ultrapure Al. The mean jump distance L at the beginning of deformation is somewhat smaller in the alloy systems compared to ultrapure Al. This can be expected since there exists an increase of the flow stress caused by the solute atoms.

Again with Friedel's hardening model as a starting point, the increase of the flow stress can be written analogous to equation (10)

$$\tau_2 = f_2^{3/2} \frac{\mu b}{l} \tag{11}$$

where l is the mean spacing of neighbouring solute atoms above or below the glide plane: $l = b/\sqrt{2c}$. In this local-force model, only those solute atoms in the two planes immediately adjacent to the slip plane contribute. Substituting the experimentally found

Table 1. Theoretical predictions and experimental observations of the effective solute spacing l_e (μm)

Alloy	Friedel equation (12)	Mott–Nabarro equation (19)	NMR equation (13)	$\dot{\epsilon}$-change equation (14)
Al–Zn (1%)	0.04	0.15	0.19	0.48
Al–Zn (1.5%)	0.03	0.11	0.16	0.32
Al–Zn (2%)	0.02	0.09	0.13	0.27

value of τ_2 into equation (11) the obstacle strength f_2 can be calculated [$\tau_2(1\%\text{Zn}) = 0.5$ MPa, $\tau_2(1.5\%\text{Zn}) = 0.7$ MPa, $\tau_2(2\%\text{Zn}) = 1$ MPa]. The average value of f_2 is 0.003, indicating that forest dislocations are strong obstacles compared to solute atoms. Analogous to equation (9), the effective obstacle spacing can be written as

$$l_e = \frac{b}{\sqrt{2 f_2 c}}. \qquad (12)$$

l_e is listed in Table 1.

A plausible connection between the effective forest dislocation spacing λ_e, the effective solute spacing l_e and the measured jump distance L_{NMR} can be based on the following model.

All moving dislocations in the alloy, delayed at intersections with both forest dislocations and solute atoms, affect the spin-lattice relaxation rate. It has to be emphasized that all delay times larger than 10^{-4} s contribute to $(T_{1\rho}^{-1})_D$. Consequently, the intersections between moving dislocations and weak obstacles like solute atoms affect the spin-lattice relaxation rate and the intersections with strong obstacles like forest dislocations influence $(T_{1\rho}^{-1})_D$. Assuming two different sets of corresponding mobile dislocation densities, ρ_1 and ρ_2, respectively, the total spin-lattice relaxation time can be decomposed into two contributions analogous to equation (8). One can envision that at the yield stress level in the case of the dilute alloy a small fraction of the primary dislocations must move through the weak obstacle field presented by the solutes before encountering forest dislocations; the effective solute spacing is much smaller than the forest dislocation spacing (Table 1). The mean jump distance L_{NMR} can be written as

$$\frac{1}{L_{NMR}} = \frac{\rho_1}{\lambda_e \rho} + \frac{\rho_2}{l_e \rho}. \qquad (13)$$

In order to verify this expression, we have to make the necessary assumption that the dislocation microstructure is the same in ultrapure Al and in the dilute Al–Zn alloys at a certain value of ϵ. In view of the method of analyzing strain-rate change experiments by Van Den Beukel *et al.* [15], this implies that a plot of L_{NMR}^{-1} vs L_{NMR}^{-1} of ultrapure Al is a straight line. In Fig. 6 L_{NMR}^{-1} vs L_{NMR}^{-1} is depicted for both the alloy systems and the pure material. At the beginning of deformation of the alloys $\rho_2/\rho \simeq 1$ (assuming the two different fractions of mobile dislocation densities are proportional to the corresponding ratios of the effective planar obstacle densities). It means that, according to equation (13), at the smallest degree of deformation ($\epsilon \simeq 1\%$) measured by NMR, l_e is found to be decreasing from 0.19 μm in Al–1 at.% Zn to 0.13 μm in Al–2 at.% Zn. From a comparison between this experimental finding and the values predicted using Friedel statistics (Table 1), it can be concluded that actually in each dislocation jump a number of effective solute atoms (order of 10) is bypassed. In steady state, Friedel statistics assume that a dislocation released at one obstacle must, on average pick up exactly one other one. This seems to be in conflict with these NMR data.

According to our assumption, λ_e is the effective separation of forest dislocations in the solid without solute atoms and has the same strain dependence in the alloy as in the ultrapure material. Further, l_e is assumed to be independent of strain. However, when primaries move through a random field of solute atoms before encountering forest dislocations, the dislocation mobility is decreased relative to that possible at the same stress level compared to ultrapure material. In order to keep up with a fixed applied strain rate $\dot{\epsilon}$ [equation (1)], the dilute alloy may have ρ_m greater than for the pure crystal. Consequently at a corresponding strain the alloy has to have a higher stress level than the ultrapure crystal. It means that the effective obstacle spacing λ_e [equation (9)] in the alloy will become smaller than λ_e observed in the ultrapure material. As a result the

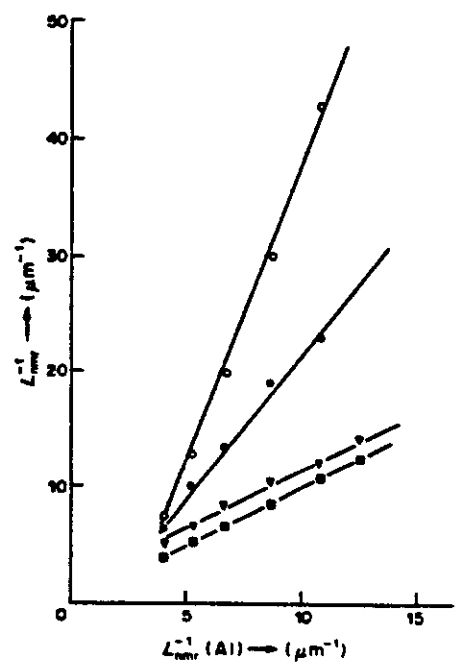

Fig. 6. Inverse mean jump distance L_{NMR} vs the same quantity of L_{NMR} in ultrapure Al (symbols see Fig. 4).

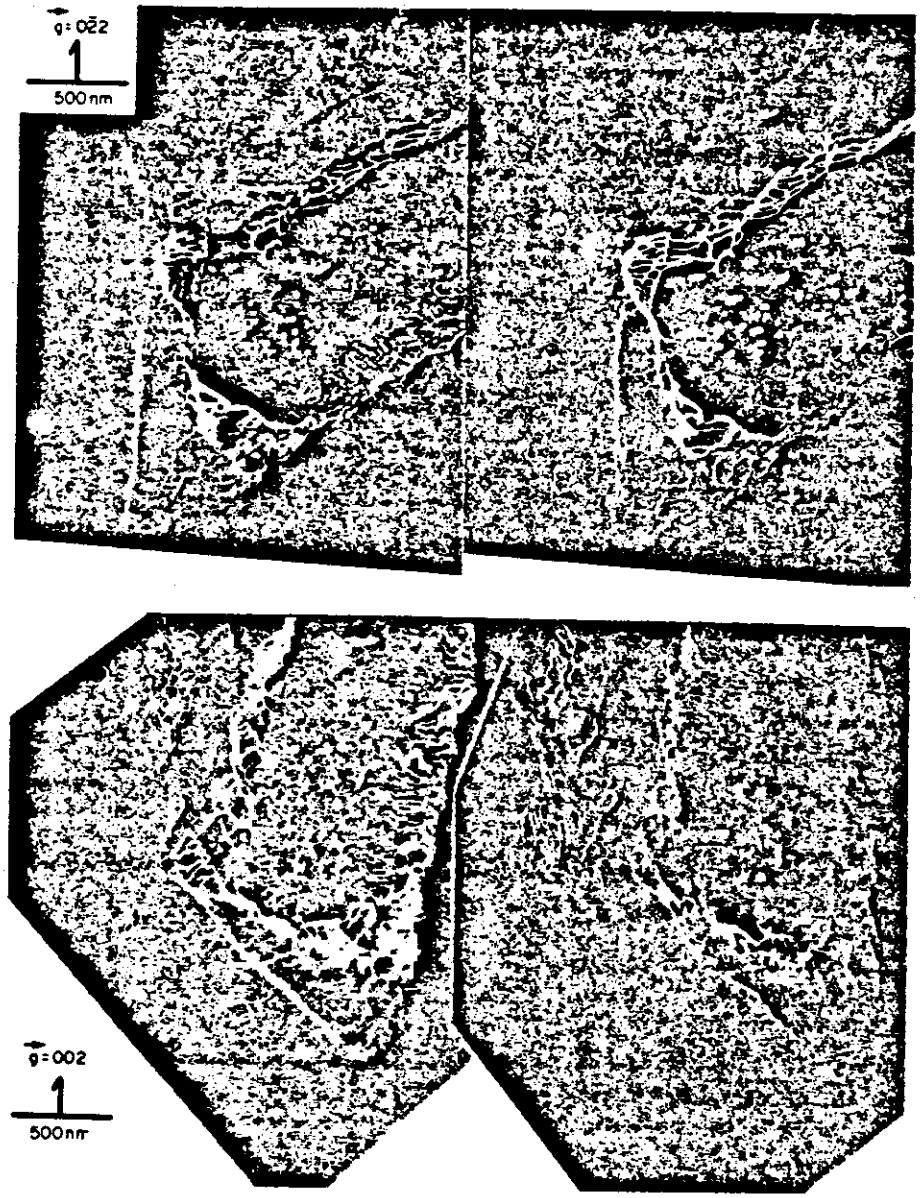

Fig. 7. Stereo-electron micrograph of Al–1 at.% Zn deformed at 77 K until fracture. (a) $\mathbf{g} = 02\bar{2}$, stereo angle 19.2°, stereo impression [311]. (b) $\mathbf{g} = 002$, stereo angle 25°, stereo impression [100].

slope of L_{NMR}^{-1} vs L_{NMR}^{-1} (Al) of the alloys will increase from one with increasing solute concentrations (see Fig. 6). At higher deformation λ_t in the alloy will become smaller than λ_t observed in the ultrapure material (see Fig. 4). This discussion ignores the effect of solutes on the stacking fault energy of aluminium (cell structure formation). TEM observations of the present dilute alloy systems show cell structures quite similar to the structure found in ultrapure Al (Fig. 7). For further discussion on the c dependence of L_{NMR} see 4.3.

4.2. *Activation length*

Mechanical tests involving a change in strain rate by a factor of ten were employed to measure $(\delta \ln \dot{\epsilon}/\delta\tau)_T$ [equation (5)], from which the apparent activation volume was deduced. The resulting data, depicted in Fig. 8, reveal that the apparent activation volume and activation length of the system decrease with increasing strain. This behaviour has been observed also in f.c.c. crystals using the same techniques, e.g. in Al by Mukherjee *et al.* [16] and in Cu by Van Den Beukel *et al.* [15]. The effective activation length represents the mean spacing of the forest dislocations [17]. The rate at which the decrease of activation length with increasing strain happens, depends on the number of operative slip systems (strain hardening). λ is expected to decrease more rapidly with strain hardening the greater the amount of (poly) homogeneous slip. Since the rate of decrease of λ with ϵ is the same among the various systems

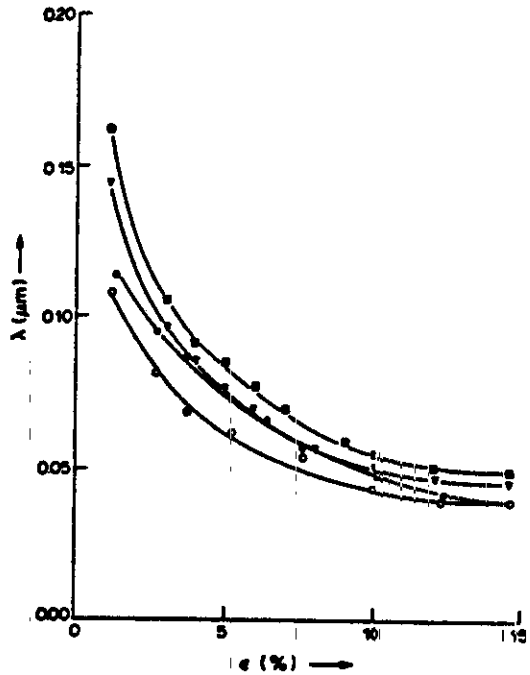

Fig. 8. Activation length determined from strain rate change experiments (symbols see Fig. 4).

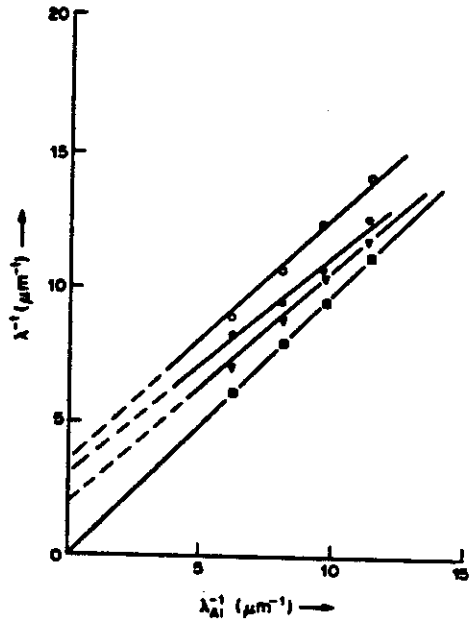

Fig. 9. Inverse activation length λ_{alloy} vs the same quantity of λ in ultrapure Al (symbols see Fig. 4).

(Fig. 8), the strain hardening associated with these experiments is expected to be the same as well.

It should be noted that, in general, the effective length is proportional to the applied stress $\tau^{-1.5}$ [13], [equation (9)]. The activation volume will become equal to $2/3\ \lambda\ b^2$ leading to a somewhat larger value of λ than depicted in Fig. 8. The activation length λ at small ϵ is close to the value of L_{max} at small ϵ.

According to Kocks [19] the resulting activation length in the case of many weak and a few strong obstacles (based on a linear additivity of flow stresses) can be written as

$$\frac{1}{\lambda_{alloy}} = \frac{c'}{\lambda_e} + \frac{1}{l_e} \qquad (14)$$

where λ_e and l_e represent the activation lengths when only forest dislocations and solute atoms, respectively, are present. The λ^{-1}_{alloy} vs λ^{-1}_{Al} plots are shown in Fig. 9. It can be concluded that relation (14) is valid for the Al–Zn alloys under investigation.

In contrast to Kock's original model ($c' = 1$) in the present system $c' \simeq 0.9$. The intercept with the ordinate has the magnitude l_e^{-1}; l_e is listed in Table 1. Again (see Section 4.1) these data obtained from strain-rate change experiments indicate that in each dislocation jump a number of effective solute atoms (order of 10) is bypassed.

In order to verify the linear additivity of inverse activation lengths and to obtain *experimental* information about the obstacle strengths f_i, λ_i we write for the flow stress

$$\tau_{alloy} = \frac{k_1}{\lambda_e} + \frac{k_2}{l_e}. \qquad (15)$$

Substitution of equation (14) into equation (15) yields

$$\tau = \frac{k_1/c'}{\lambda_{alloy}} + \frac{k_2 - k_1/c'}{l_e} \qquad (16)$$

at constant l_e, and

$$\tau = \frac{k_2}{\lambda_{alloy}} + \frac{k_1 - c'k_2}{\lambda_e} \qquad (17)$$

at constant λ_e. k_i is equal to $f_i\ \mu b$ [f_i is obstacle strength of type i, see equations (9), (10), (11)].

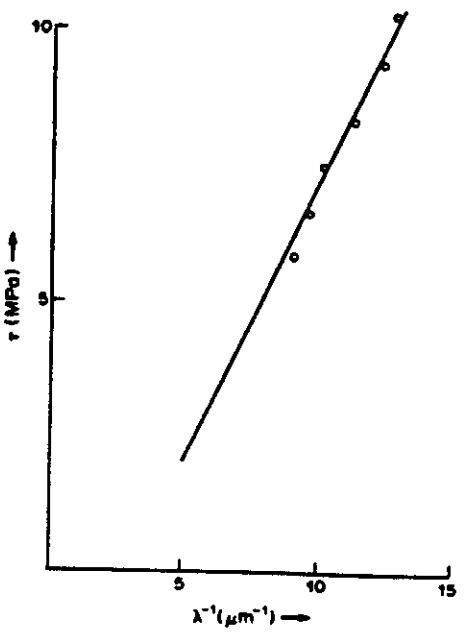

Fig. 10. Flow stress τ (Al–2 at.% Zn) vs the inverse of the activation length λ_{alloy}.

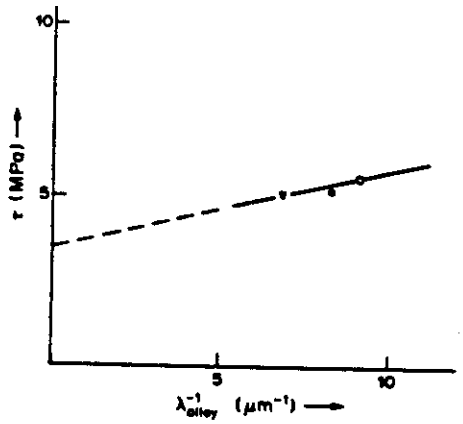

Fig. 11. Flow stress at $\epsilon = 1\%$ strain is plotted vs the inverse of the activation length λ_{alloy} (symbols see Fig. 4).

In Fig. 10 τ is plotted vs λ^{-1}_{alloy} (Al: 2 at.% Zn). According to equation (16) f_1 is found to be 0.13 and f_2 is 0.043 derived from the slope and the intercept respectively. In this analysis l_c was taken from Fig. 9: 0.27 μm for Al: 2 at.% Zn. Although only three different alloys were investigated, τ at $\epsilon = 1\%$ strain is plotted vs the inverse of the activation length λ^{-1}_{alloy} in Fig. 11. Using equation (17) f_2 is found to be 0.035 and f_1 is 0.11 ($\lambda_c = 0.16\ \mu$m, Fig. 8). The assumption that the forest dislocations are strong obstacles compared to the solute atoms seems to be justified. The strain-rate change experiments confirm the linear additivity of flow stresses and the additivity of inverse activation lengths.

4.3. Comparison between mean jump distance and activation length

In conclusion we may say that there exists mutual consistency between the mean jump distance measured by NMR and the activation length obtained by strain-rate change experiments. It has to be emphasized that L_{NMR} is obtained from samples which are deformed with *constant strain rate* $\dot{\epsilon}$ with increasing stress. This means that L_{NMR} is dynamically influenced dislocation multiplication. *Changes in strain rate* during deformation, however, can cause similar effects to the flow stress as changes in temperature. An increase in strain rate gives less time for thermally activated events: i.e. it is equivalent to a lowering of the temprature of deformation. In addition, the cooperative way of dislocation dynamics will affect the activation length. A dislocation pinned at different obstacles may "unzip" along its entire length after thermal activation of only one segment of the dislocation across the barrier, since at that very moment the critical breakaway angle of all other segments is exceeded. Only a small activation length per segment would be measured, although L_{NMR} in that case need not be influenced by this unzipping effect. The difference between L_{NMR} and λ_{alloy} is most clearly indicated by the different effects of solute concentration on the strain dependence (Fig. 6, Fig. 9). Apparently, the rate at which the decrease of L_{NMR} with increasing strain happens, depends considerably on the concentration c of solute atoms (Fig. 4, Fig. 6) and is proportional to the strain hardening, θ (in stage II $1/L \sim \theta^2\,\epsilon$).

According to equation (10)

$$\theta = \frac{\delta\tau}{\delta\gamma} = \frac{\alpha\mu b}{2\sqrt{\rho}}\frac{\delta\rho}{\delta\gamma}. \tag{18}$$

The rate of change of dislocation density with strain is $1/bL$. A detailed analysis [20] of the strain hardening behaviour indicates that the presence of solutes does not greatly affect the dislocation accumulation. It means that the increase of the slope L^{-1}_{NMR} vs $L^{-1}_{(Al)}$ (Fig. 6) with increasing c is due to an increase of the strength of dislocation/dislocation interaction α; i.e. surprisingly enough, there exists some arrangement of solutes correlated with the position of the dislocations which can occur even at this rather low temperature that results in an increase in the effective dislocation/dislocation strength. Recently, this multiplicative effect of solutes on strain hardening has been found in Ni–Mo alloys as well [21]. For an overview of the effects of solutes on the strain hardening behaviour of alloys reference is made to [22].

Both the NMR data and the data obtained from strain-rate change experiments on the alloy systems indicate that Friedel's approximation of solution hardening is violated: i.e. in each dislocation jump a number of effective solute atoms (order of 10) is bypassed. Applying Mott–Nabarro's model as a different approach [2, 3, 23], we take the effective obstacle spacing as

$$l_c = \left(\frac{4\mu b}{\tau_i l}\right)^{2/3} l \tag{19}$$

where the maximum internal stress averaged over the space of radius $l/2$ around each solute is (see also Labusch [24, 25]).

$$\tau_i \simeq \mu\,|\delta|\,c \ln 1/c. \tag{20}$$

δ represents the misfit parameter ($\simeq 0.02$) and in the localized-force model l is related to the atomic fraction concentration c of solute by $l = b/\sqrt{2c}$. From equation (19) l_c is calculated and listed in Table 1. These predicted values are in reasonable agreement with experiments.

5. CONCLUSION

Pulsed nuclear magnetic resonance is shown to be a complementary new technique for the study of moving dislocations in Al–Zn alloys. Spin-lattice relaxation measurements clearly indicate that fluctuations in the quadrupolar field caused by moving dislocations in Al–Zn are different from those in ultra pure Al. The NMR experiments provided information on the mean jump distance of dislocations in these materials. The mean jump distance found in ultra pure Al can be explained using Friedel's model

for describing the interaction between moving dislocations and forest dislocations. Based on the NMR data and data obtained from strain-rate change experiments it could be concluded that moving dislocations interact with solute atoms as described by Mott–Nabarro's model and with forest dislocations as predicted by Friedel's model. In fact, only fairly strong obstacles at very low concentrations ($c \simeq 10^{-3}$) seem to fall inside the range where Friedel's model is justified [9]. Forest dislocations are probably a borderline case. In contrast Labusch [24], presenting a more complete solution of the statistical problem of hardening, finds that Friedel statistics are rarely justified. A more complete discussion about these various models of solution hardening is presented in a recent review by Nabarro [23].

Acknowledgements—This work is part of the research programme of the Foundation for Fundamental Research on Matter (FOM-Utrecht) and has been made possible by financial support from The Netherlands Organization for the Advancement of Pure Research (ZWO-The Hague) and the Deutsche Forschungsgemeinschaft, F.R.G.

REFERENCES

1. E. Orowan, *Z. Phys.* **89**, 634 (1934).
2. F. R. N. Nabarro, In *The Physics of Metals II. Defects* (edited by P. B. Hirsch), p. 152. Cambridge Univ. Press, (1975).
3. F. R. N. Nabarro, *Phil. Mag.* **35**, 613 (1977).
4. J. Th. M. De Hosson, O. Kanert and A. W. Sleeswyk, *Dislocations in Solids* (edited by F. R. N. Nabarro), Vol. 6, Chap. 32, pp. 441–534, North Holland, Amsterdam (1983).
5. H. Tamler, O. Kanert, W. H. M. Alsem and J. Th. M. De Hosson, *Acta metall.* **30**, 1523 (1982).
6. H. J. Hackelöer, O. Kanert, H. Tamler and J. Th. M. De Hosson, *Rev. scient. Instrum.* **54**, 341 (1983).
7. J. Th. M. De Hosson, A. J. Huis in't Veld, H. Tamler and O. Kanert, *Acta metall.* **32**, 1205 (1984).
8. O. Kanert and M. Mehring, *Statistic Quadrupole Effects in Disordered Cubic Solids, NMR*, Vol. 3, p. 3. Springer, Berlin (1971).
9. U. F. Kocks, A. S. Argon and M. F. Ashby, *Progress in Materials Science* (edited by B. Chalmers, J. W. Christian and T. B. Massalski), Vol. 19, p. 1. Pergamon Press, Oxford (1975).
10. U. F. Kocks, In *Fundamental Aspects of Dislocation Theory* (edited by A. Simmons, R. DeWit and R. Bullough) Vol. 2, p. 1077. NBS Spec. Publ. 317 (1970).
11. A. D. Le Claire, *J. nucl. Mater.* **69 & 70**, 70 (1978).
12. N. L. Peterson, *J. nucl. Mater.* **69 & 70**, 3 (1978).
13. P. B. Hirsch, In *Physics of Metals, II Defects* (edited by P. B. Hirsch), p. 189. Cambridge Univ. Press (1975).
14. Z. S. Basinski, *Phil. Mag.* **40**, 393 (1959).
15. G. J. Den Otter and A. Van Den Beukel, *Physica status solidi.* (a) **55**, 785 (1979).
16. A. K. Mukherjee, J. D. Mote and J. E. Dorn, *Trans. metall. Soc. A.I.M.E.* **233**, 1559 (1965).
17. A. Seeger, *Dislocations and Mechanical Properties of Crystals*, pp. 243–332. Wiley, New York (1956).
18. J. Friedel, *Dislocations*. Pergamon Press, New York (1964).
19. U. F. Kocks, *Trans. Japan Inst. Metals* **9**, 1 (1968).
20. M. J. Luton and J. J. Jonas, *Can. Metall. Q.* **11**, 79 (1972).
21. T. A. Bloom, U. F. Kocks and P. Nash, *Acta metall.* **33**, 265 (1985).
22. C. G. Schmidt and A. K. Miller, *Acta metall.* **30**, 615 (1982).
23. F. R. N. Nabarro, In *Dislocations and Properties of Real Materials*, p. 152, Inst. Metals, London (1985).
24. R. Labusch, *Acta metall.* **20**, 917 (1972).
25. R. Labusch, *Physica status solidi.* **41**, 659 (1970).